KØBENHAVNS UNIVERSITET
&
UNIVERSITÄT HOHENHEIM

MASTER THESIS

# Holocene Climate and Ice Flow of the Renland Ice Cap

*Author:*
Sonja WAHL

*Supervisors:*
Bo Møllesøe VINTHER
Kirsten WARRACH-SAGI

*A thesis submitted in fulfillment of the requirements*
*for the degree of Master of Science*

*at*

Centre for Ice and Climate
Niels Bohr Institute

30 ECTS Thesis
March 15, 2018

KØbenhavns Universitet
&
Universität Hohenheim

# *Abstract*

Centre for Ice and Climate
Niels Bohr Institute

Master of Science

**Holocene Climate and Ice Flow of the Renland Ice Cap**

by Sonja WAHL

Measured ice core borehole temperatures contain valuable information about climatic conditions of the past. Numerical borehole temperature models are the tool for extracting this information, allowing the reconstruction of past temperatures. Profound knowledge about the ice flow is required when developing a borehole temperature model.
This thesis aims to reconstruct the Holocene temperature history of the Eastern Greenlandic peninsula Renland which is of use for estimating the future Greenland Ice Sheet behaviour in a changing climate.
Borehole temperature models were set up for two ice core drill sites located in close proximity to each other on the Renland Ice Cap. The models reproduce the observed ice cap temperature profiles within an accuracy of 0.03 °C. A new concept referred to as *step-model* was introduced to describe the ice flow at the two locations. It is supported by comparing model results with observed annual layer thicknesses and ice age markers. Surface temperature reconstruction was performed using temperature records from remote weather stations as well as $\delta^{18}$O isotope proxy data. Both methods calculate similar temperatures for the 20$^{\text{th}}$-century, revealing a mid-century warming and a steep increase in temperatures since 1980. Holocene temperatures were reconstructed by calibrating an isotope paleothermometer. The resulting temperature estimates agree in their overall pattern and indicate a climatic optimum around 9 ky b2k with an apparent and mostly steady cooling trend thereafter.
The developed borehole temperature models are limited in their temporal validity, but demonstrate the feasibility to model temperature profiles of the Renland Ice Cap. They can be further modified to extend their validity into the glacial, allowing temperature reconstructions of the entire ice core record, dating back into the Eemian.

# *Acknowledgements*

Weil einfach ja langweilig wäre...
Writing your master thesis at a physics department without being a physicist might sound overly-ambitious and needlessly complicated to some students. For me, it was the best decision I could have made. I learned loads, got insight into really exciting science and met a lot of interesting people. The Centre for Ice and Climate with its coffee smell and the friendly atmosphere is responsible for me handing in my thesis today, without being overworked or tired of university. I have to thank Brice Noël from IMAU, Utrecht University, who kindly processed and provided the RACMO2.3 data set and DMI for providing the HIRHAM5 data set. Looking back after half a year of thesis work, I want to mention some people explicitly and thank them for their support.
First and foremost, *Tak* Bo, for the (almost) weekly meetings, your encouragement and for never being tired of answering my questions, even if the answers were sometimes obvious. You were the one who introduced me to ice core glaciology with such enthusiasm, that I was immediately infected. *Danke Dir* Kirsten, for being so interested and supportive despite the additional workload. *Tak* Iben, for always having an open door and explaining all the little things, which are important to know besides the physics. *Bedankt* Santosh, for coffee walks and honesty. I am grateful for the many who have read or offered to read this thesis and their revisions. I acknowledge the improvement of my work through their help. I also want to thank the other master students in RF 305 who created an enjoyable working atmosphere. Having someone to talk to really improved my mood. A big *thank you* to my flatmates! I appreciated coming home to friends more than anything else during the writing phase. And lastly, *Danke* to my family, my boyfriend and my friends who supported me from afar for the encouragement, unlimited patience and the right words at the right time.

# Contents

# List of Figures

# List of Tables

# Chapter 1

# Introduction

## 1.1 Climate and ice

### 1.1.1 The cryosphere in the climate system

Earth's climate is not in a stable state and has never been. The planet has experienced cold climate stages, called *glacials* as well as warm *interglacial* periods, intermitted by transitional phases. The glacial-interglacial cycle has a period of roughly 100,000 years and paleotemperature reconstructions estimate corresponding temperature differences of >10°C for the polar regions (Petit et al., 1999; Vinther et al., 2009b). Currently, the Earth is in a warm period, called the Holocene, which began around 11,700 years ago (Rasmussen et al., 2006)
A change in climate will always induce a change in the Earth's appearance and vice versa since the climate system is dependent on several components of the planet. The climate system is defined as the interaction of the atmosphere, the hydrosphere, the lithosphere, the biosphere and the cryosphere, which are all coupled by various interdependencies and feedbacks. The external forcing driving the climate system is the sun. (Intergovernmental Panel on Climate Change, 2014).
The cryosphere is defined as all solid-phase water on earth. This includes permafrost, frozen lakes, snow, mountain glaciers, icebergs and sea ice as well as the two ice sheets currently existing. The latter contain more than 99% of the freshwater on Earth. One is the *Antarctic Ice Sheet* with an area of almost $14{\cdot}10^6$ km$^2$. The other one is the *Greenland Ice Sheet* with an extent of about $1.7{\cdot}10^6$ km$^2$ (Alley et al., 2010). In general, the Greenland Ice Sheet experiences higher accumulation rates and warmer temperatures compared to the Antarctic Ice Sheet with mean annual temperature of -30°C and accompanying low accumulation rates below 80 mm water equivalent per year (Casado et al., 2016). The cryosphere, like any other climate system component, is subject to climate forcing and feedbacks and its extent has varied over time (Alley et al., 2010). The behavior of ice sheets in a changing climate is of high interest, as a recent warming of the planet has been recorded and further warming is predicted. The reaction of the cryosphere, and ice sheets in particular, to a warming climate might have significant global socioeconomic and human health effects. Sea level rise and reinforced warming are two examples of it. Ice core glaciology is an important part of paleoclimatology. In this field of climate research the past

behaviour of the climate system is analysed in order to understand and therefore be able to make predictions about climate trends in the future.

### 1.1.2 Climate proxies in ice with time scale

Information about past climatic conditions, qualitative and even quantitative can be found in what science calls *proxies*. Those are natural archives that carry information about past climates because of their dependency on one or more climatic parameters. As soon as the relationship and its behaviour is understood, the signals in the archives can be translated into climate records. Besides others, ice cores, drilled on ice sheets or glaciers contain such proxies and can yield climatic records dating back several thousand years. The oldest ice currently known is ice from the DOME C drill site in East Antarctica, closely followed by DOME F, being dated to be 800 kyears and 720 kyears old, respectively (Jouzel et al., 2007; Kawamura et al., 2017). Ice cores from Greenland reach about the same length as Antarctic cores, however as accumulation rates are significantly higher in Greenland and some locations experience basal melt, ice at bedrock is not as old in Greenland. The oldest continuous record at NGRIP was dated to be 123 kyears old, i.e. reaching into the last warm period, the Eemian (Rasmussen et al., 2006). Even older ice, likely from before the Eemian, was discovered at NEEM (NEEM, 2013). However, exact dating is difficult due to layer folding close to bedrock. Accurate proxy analysis is only possible if good dating of the proxy carrier is provided.
Dating of ice cores is possible by annual layer counting in the top section, as well as impurity and isotope measurements for dating of older ice and matching those references to an universal timescale, e.g. the GICC05 (Rasmussen et al., 2006). This way, all ice core records, transferred to the same timescale, can be compared.
Impurities present in the ice core originate from deposits on snow and are hence absorbed into the emerging ice column. Examples are particles from volcanic eruptions being dispersed through the atmosphere as well as dust coming from various sources. Alternations in impurity concentrations can be detected by electrical conductivity measurements since conductivity in ice is related to its purity and the composition of the trapped particles. Identified prominent layers can then be linked to known reference points in time, e.g. volcanic eruptions. Moreover, stable isotope analysis is performed on ice cores. The heavy isotopologue - abundant isotopologue relationship can be used to translate isotopologue concentrations in precipitation as well as temperature signals. Additionally, gas analysis of air bubbles, trapped in the ice, reveal past atmospheric gas compositions. Ice crystal structure carries information about the prevailing stress conditions and deformation processes, the ice had undergone earlier. Merging all research results together enables a reconstruction of past climatic conditions. Taking into account knowledge, retrieved from multiple climate proxies can enable a deeper understanding of the Earth's climate system

and the way it responds to various forcing. It is therefore of greatest interest to understand the climatic behavior of the past, to make reasonable predictions about the future.

## 1.2 Renland and the RECAP project

So far, six deep drilling projects were conducted on the main Greenland Ice Sheet: Camp Century, DYE3, GRIP, GISP2, NGRIP, NEEM (Gundestrup et al., 1993; Dahl-Jensen, 1998; Grootes et al., 1993; Dahl-Jensen et al., 2003; NEEM, 2013). Besides those multi-annual drill projects, smaller ones have been carried out in Greenland as well. The small Renland Ice Cap in eastern Greenland was chosen for two one-season drill projects. One core was drilled in 1988 and a new one in 2015 in proximity to the first (Johnsen et al., 1992; *The REnland ice CAP project (Sapere Aude)*). Analysing, interpreting and modelling the borehole temperature curves of those two field campaigns is done in this thesis.

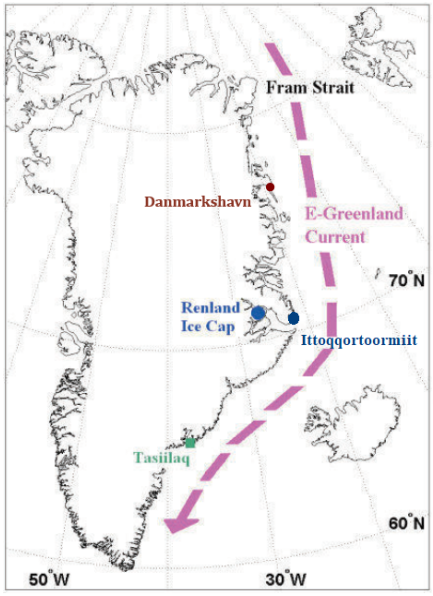


FIGURE 1.1: **Map of Greenland**
The Renland peninsula is marked as well as the locations of the three DMI weather stations Ittoqqortoormiit, Danmarkshavn and Tasiilaq. (*The REnland ice CAP project (Sapere Aude)*).

### 1.2.1 Renland

Renland is a peninsula, situated in Eastern Greenland in the Scoresbysund Fjord with a bedrock elevation of roughly two kilometers (Figure 1.1). Taking the ice cap, that sits on the peninsula, into account, the surface elevation sums up to a 2340 m high summit. The extend of the ice cap is constrained by the limits of the plateau whose margins are steep. The fjords's outreaches surround the peninsula almost

completely and drain the ice cap efficiently. Hence the ice cap is isolated from the main ice sheet, which was the case throughout the entire Holocene. This also leads to the assumption that the ice cap height has been more or less constant since the end of the last glaciation (Johnsen et al., 1992). Due to its proximity to the sea, Renland's climate is highly influenced by the East-Greenland current carrying arctic waters southwards along Greenland's shore. The climate on the peninsula has never been recorded long-term. However, Danish Meteorological Institute (DMI) weather stations on the coast some 600 km north- and southward have been run since the early 20$^{th}$ century and can give hints to recent climate development in Eastern Greenland.

### 1.2.2 Renland Ice Cap project

The Renland Ice Cap has been subject to scientific interest since the 1980's. Because of its limited ice cap height of maximum 600 m, the proximity to the sea and high accumulation rates of roughly 0.5 m ice equivalent/year the ice sheet was chosen for drill campaigns twice. During the first field season in 1988, a 324 m long ice core was drilled using dry drilling techniques (Johnsen et al., 1992). It can be seen as the shorter red line on the radar echogram in Figure 1.2. Due to dry drilling

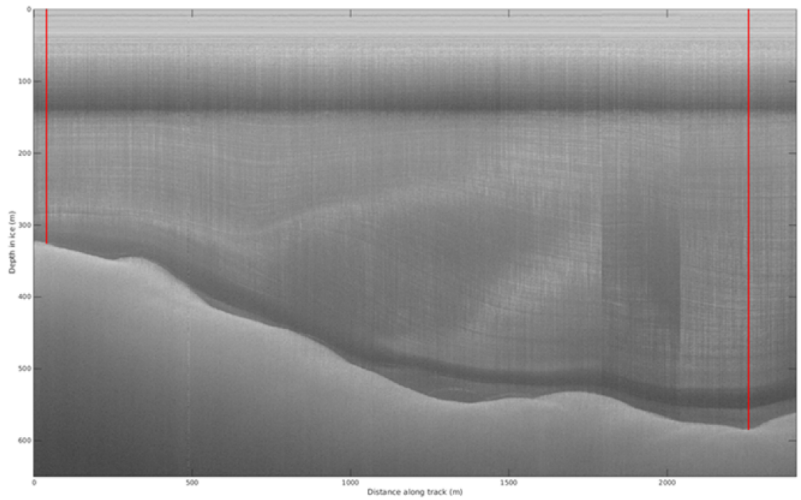


FIGURE 1.2: **Radar echogram of Renland drill sites** The two red lines indicate the location of the drilled cores. The site of the old, shorter borehole from 1988 can be seen as well as the site of the new RECAP core from 2015. (Team Radar RECAP 2015).

techniques, the quality of this ice core is 'rather poor', compared to recent standards and neither gas nor continuous chemical analysis have been performed on it (Bo Vinther, CIC). Discrete sampling measurements are available for the whole length of the ice core. A second drilling was conducted between April and June in 2015 roughly two kilometers away from the old core from 1988. The project was called the *Renland Ice Cap project*, short *RECAP*, and the location for the core was chosen by radar measurements. The bedrock topography of the area around the summit and the two drilling locations can be seen in Figure 1.3. Only the location of the Renland

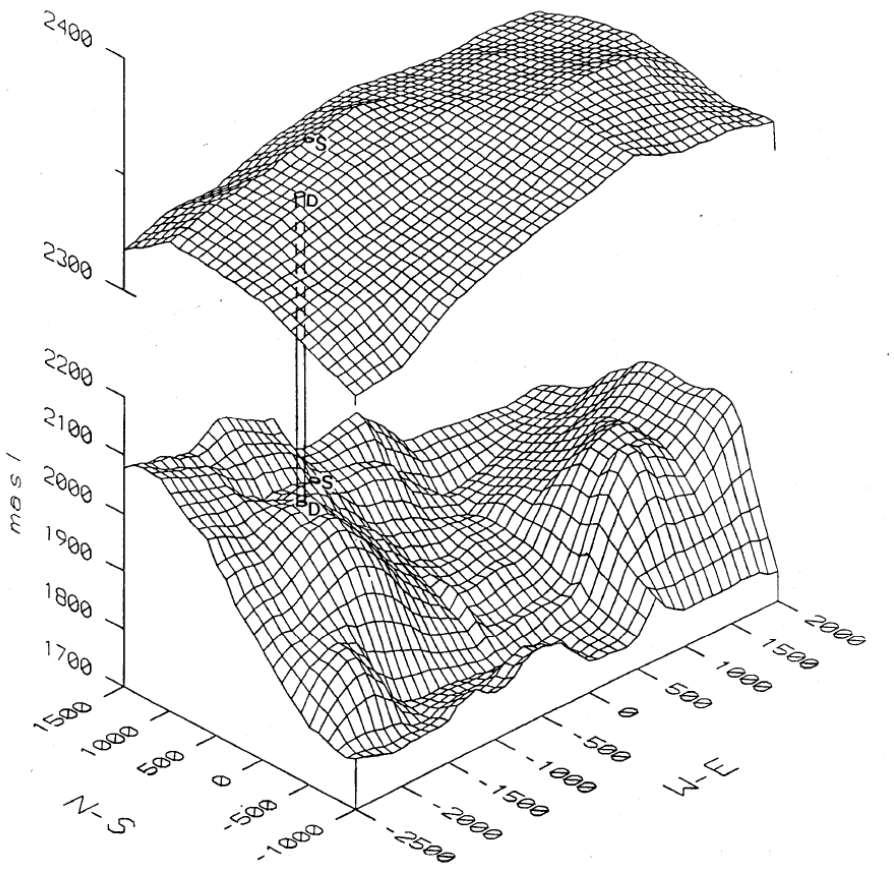


FIGURE 1.3: **Surface and bedrock topography around the drilling locations**
The borehole location from 1988 (D) can be seen as well as the valley, in which the core from 2015 was drilled. From Johnsen et al. (1992).

1988 core is indicated. A 584 m long ice core was drilled to bedrock in the valley east of the old drill site in 2015.

The RECAP core contains a full record of the last glacial as well as even older ice, likely from the last warm period, the Eemian dating back to roughly 125,000 years (*The REnland ice CAP project (Sapere Aude)*). Table 1.1 contains the most important facts of the two drilling projects that were carried out on the Renland Ice Cap.

TABLE 1.1: The Renland drilling campaigns - facts

| | **latitude** °N | **longitude** °W | **elevation** m | **date** | **core length** m |
|---|---|---|---|---|---|
| Renland 1988 | 71.3064 | 26.7681 | 2340 | 07/1988 | 324 |
| RECAP | 71.3036 | 26.7132 | 2331 | 04-06/2015 | 584 |

## 1.3 Aim of this thesis

### 1.3.1 Ice Core Borehole Temperatures

Ice core borehole temperatures are of high value in ice core research. They allow the reconstruction of paleotemperatures from isotopes, can asses the effectiveness of Regional Climate Models (RCM) and give insight in recent surface temperature developments. Apart from the use of borehole temperatures as a method to analyse climate they are helpful for ice sheet modelling. It is a necessity to know the temperature distribution throughout an ice sheet when modelling the dynamics of ice sheets or ice caps. The temperature of the ice impacts ice flow and vica versa (Cuffey and Paterson, 2010). Previous studies have modelled borehole temperatures of GRIP and DYE-3 in order to reconstruct paleotemperatures 50 kyears and 7 kyears back in time, respectively (Johnsen et al., 1995; Dahl-Jensen, 1998; Dahl-Jensen, 1998). The successful modelling of borehole temperature curves (BTCs) for Camp Century, DYE-3, GRIP and NGRIP validated Vinther et al. (2009a)'s Greenland ice sheet elevation change calculations.
A successful borehole temperature model (BTM) requires prerequisite information on density, ice flow and heat transfer understanding of the ice sheet at the drill location. This thesis aims to set up:

- An ice flow model which describes the vertical thinning of the annual layers. Known age markers (ice age at a specific depth) will be used to fit a model
- A density model which simulates the densification process in agreement with ice core density measurements
- A numerical heat conduction model, which incorporates the above mentioned models and calculates temperature profiles, close to observed borehole temperatures

for both Renland drill sites. Model differences between the two sites will be outlined and the resulting curves discussed. Apart from ice sheet characteristics, the model requires site specific surface temperature forcing. Data from three Danish Meteorological Institute (DMI) stations will be used and compared against each other. The aim is to find an universal temperature history for Renland of the past century, that models the observed BTCs reasonably well. With this, assumptions can be made about the past prevailing climatic conditions at Renland.

Having a valid BTM in place two different RCMs will be tested for their performance in the Renland area. The evaluated RCM are the polar versions of the RACMO and HIRHAM RCM. Eventually, the BTMs will be used to calibrate an isotope paleothermometer. The concept of this paleothermometer is a strong linking between the isotopic signal in precipitation and the prevailing surface temperature (Dansgaard, 1964). In describing this dependency through a linear relationship, the $\delta^{18}$O-isotope records of the two ice cores can be used as BTM surface forcing. The formula that best describes the linear relationship is gained through matching modelled and observed BTCs. The now calibrated paleothermometer will then be used to reconstruct paleotemperatures of the Holocene period from the two Renland isotope records. Analysis of the Holocene temperature records will be performed to see, if they tie in with other temperature reconstructions of that area or indicate an outstanding climate behaviour. In this thesis the following research questions will be addressed:

- How can the ice flow at the Renland Ice Cap summit be characterised?
- How has the temperature at Renland behaved throughout both the Holocene and the last century?
- Is the BTM method expedient for temperature reconstructions of regions without temperature records?

### 1.3.2 Thesis structure

- CHAPTER 1- INTRODUCTION
  The motivation behind the modelling of borehole temperatures is presented. Furthermore, the Renland 1988 drill campaign as well as the RECAP project from 2015 are described.

- CHAPTER 2- GLACIOLOGICAL BASICS
  The fundamental principles that are necessary for the simulation of borehole temperatures are described and explained. Ice sheet dynamics including the flow behavior as well as the compaction of snow to ice are outlined. Heat conduction processes within ice sheets are presented. Furthermore a short introduction to isotopes as temperature proxy is given.

- CHAPTER 3- MODELS, METHODS AND DATA
  The models that are used in this work to calculate the earlier introduced principles are presented. The Herron-Langway model is chosen for the densification process. The ice flow is modelled with a new modified Dansgaard-Johnsen model and a non-steady state numerical model is used for the simulation of heat conduction within the ice sheet. Moreover, the temperature datasets, that are necessary for the borehole temperature modelling are described and compared against each other. Those stem from three Greenland weather stations as well as two Regional Climate Models. Finally, the $\delta^{18}O$-isotope dataset, which is later analysed to calculate a temperature-isotope dependency, is presented.

- CHAPTER 4- RESULTS
  The best model outcomes for the above mentioned processes are presented. The densification model that fits the density observations at both drillsites is shown. Further, the assumptions that lead to a best age-fitted flow model are described. Both are then used to model the BTCs. The results of the various surface temperature forcing scenarios are presented. The identified linear ice core isotope-surface temperature relationship for both drill sites is given.

- CHAPTER 5- DISCUSSION
  The validity of the presented borehole temperature models is discussed. Different upper boundary forcing scenarios are compared and the results interpreted. The performance of the RCMs at the drill site locations is discussed. The found isotope-temperature relationship is compared against other literature. Finally, the two borehole temperature models and their results are analysed for similarities and discrepancies and subsequently interpreted.

- CHAPTER 6- CONCLUSION
  The last part of this thesis outlines the consequences of the findings for the Eastern Greenland climate. Further, borehole temperature modelling, as a method to study past climate changes, is evaluated in this context.

# Chapter 2

# Basic Glaciology

## 2.1 Glacier and ice sheet dynamics

Once a perennial ice mass has established itself, it follows simple mass balance laws: If more snow is falling onto so called *accumulation zones* than ice is melt in the *ablation zones*, the ice sheet grows, and vice versa. The allocation of the ablation and accumulation zone is variable and is influenced by latitude, altitude and solar radiation. This is valid for all kinds of ice masses, e.g. ice sheets, ice caps and glaciers. Depending on the location of the ice sheet or ice cap, ice calving can play a crucial role as a negative component in the ice sheet mass balance. Calving occurs along coastlines, when parts of the ice that are pushed over the edge break apart from the ice sheet and become drifting icebergs. Therefore, an ice cap, sitting on top of a limited solid earth area, is somehow limited in its extents and size. However, it is constantly in motion. Although being in solid phase, ice is a rather viscous material,

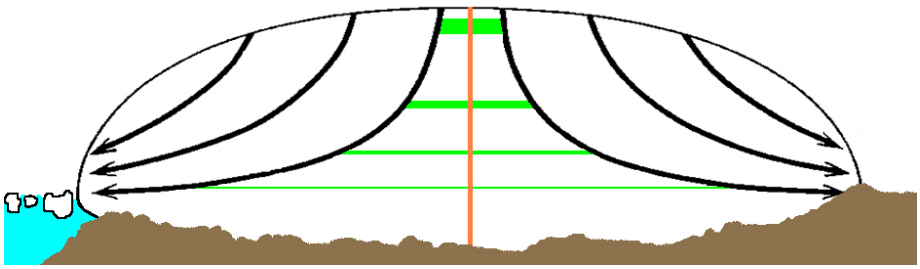

FIGURE 2.1: **Cross section of an idealised ice sheet**
The vertical line resembles the ice divide, whereas the black arrows indicate possible flow lines within the ice sheet. (Rasmussen et al., 2006).

*flowing* and deforming due to load and gravity. The high viscosity of ice, allows for slow movements only but nevertheless it flows in both horizontal and vertical directions. Following a snow parcel after deposition on an ice-sheet and ice-conversion, it will steadily sink down while being transported towards the ice margins (Figure 2.1). With this, accumulation layers traveling down through an ice sheet, will become thinner. Snow falling directly on the ice divide, resembling the dividing line for ice flowing in one or the other direction, behaves differently. It will undergo only minimal horizontal displacement, therefore travelling vertically downward, while

being thinned with a velocity relative to new accumulation being deposited on top. Hence, the accumulation rate is strongly correlated with the vertical velocity below the ice divide. Given that ice flow is well understood, an accumulation signal can be retrieved from the individual layer thicknesses. In Figure 2.1 the flow lines of ice can be seen on an idealised ice sheet as well as the ice divide.

## 2.2 Ice formation

The origin of all ice sheet ice on earth is snow. The transition zone, where snow becomes ice is described as firn. This process is driven by new snow accumulating on top of the already existing snow and compacting the layers below i.e. the load on top. Fresh snow densities ($\rho$) vary from location to location depending on the surrounding climatic conditions. Values for freshly fallen snow reach from $\rho$=50 – 70 $\mathrm{kg/m^3}$ (Cuffey and Paterson, 2010). Shortly after settling ($\rho$=200 – 300 $\mathrm{kg/m^3}$), the density of the snow layer increases due to mechanical effects that remove the spires while the ice crystals become a more rounded shape and slide closer ($\rho$=300 – 400 $\mathrm{kg/m^3}$). From here, the densification process can be divided in three stages. The first stage is driven by physical compaction and settling until a density of $\rho$=550 $\mathrm{kg/m^3}$ is reached. This is referred to as the *critical density* from where no tighter packing of grains is possible. The corresponding depth is called *critical depth* and varies from site to site, usually located within the uppermost 20 m of a firn column. It follows the second stage of densification from 550 $\mathrm{kg/m^3} < \rho <$ 820 $\mathrm{kg/m^3}$. The dominant densification process here is *sintering*, i.e. the crystallisation and deformation of ice crystals in order to lower pressure stresses. With a density of 820 $\mathrm{kg/m^3}$, the *close-off density / close-off depth* is reached. The snow has now turned into ice. Air, hitherto being able to propagate and diffuse through channels in the firn, is now trapped in air bubbles and *closed off*. Further compaction is only possible by compressing these air bubbles in the so called *creep*-zone, until constant ice density of $\rho$=917 $\mathrm{kg/m^3}$ is reached. In Greenland, close-off densities have been observed in depths between 60 to 80 m (Herron and Langway, 1980). The close-off depth is an important parameter in air bubble gas analysis. The age of the ice at close-off, relative to the age of the air trapped in the gas bubbles is called $\Delta$-age and has to be considered when interpreting gas measurements.

## 2.3 Ice - a moving substance

When describing the flow of ice, it has to be kept in mind that ice is a fluid with a very high viscosity of about $10^4$ sPa (-10°C) (Cuffey and Paterson, 2010). Impurities, like dust or other depositions, lead to viscosity alterations which affect the flow. Ice from the glacial cold periods is in general softer than ice formed during warm periods, because impurities are deposited in higher amounts relative to the low accumulation rates during glacial periods. Additionally, the ice temperature further

defines the viscosity. Friction occurring during ice movement might warm the ice, which then increases the velocity and favours ice movement. Despite those viscosity deviations within an ice mass, the ice flow has been described with some general laws.

The effect of flow of ice is foremost the redistribution of mass. It is dependent on numerous aspects of different scales. On the small scale, the ice crystal structure plays a crucial role for the ice flow. Depending on the c-axis orientation of ice crystals (normal direction relative to basal plane), one direction of flow (*easy glide*) might use less force than another direction (*hard glide*). In general, stress perpendicular to the c-axis orientation will result in higher ice deformation/movement as can be seen in Figure 2.2. However, neighbouring ice crystals are not necessarily oriented the same

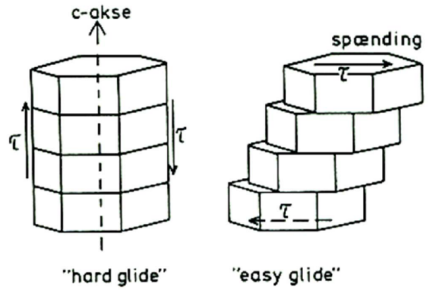


FIGURE 2.2: **Deformation of an ice crystal**
Depending on the direction the stress is implied, it will result in more (*easy glide*) or less (*hard glide*) deformation.
(lecture material Hvidberg).

way, hence an empirical formula was developed using lab experiments to describe a universal flow law called *Nye flow law* (Nye, 1952).

On the larger scale, the ice flow is dependent on the bedrock topography. It is seen in radar echograms (where individual flow lines can be seen due to differences in ice properties), that uneven bedrock topography results in folding of the ice layers above. Moreover the bedrock can be tilted or undulated which influences the gliding of the ice. In general, gravity pulls the ice mass vertically downward implying horizontal movement due to a sloping bedrock and/or resulting pressure gradients (Cuffey and Paterson, 2010). This is called the *driving stress* forcing the ice in one direction. Counteracting this is *basal resistance* resulting from bedrock characteristics and defined as the shear stress across the ice mass-bedrock contact area. Additionally ice internal mechanisms, like the creep deformation of ice slows down the movement. The deformation is a result of shear stresses near ice margins and bedrock. However those shear stresses even impact distant ice due to its almost plastic character. For the purpose of the static equilibrium assumption, those forces balance each other. However, this does not imply, that the ice mass is at rest, but rather assumes that the acceleration caused by the glaciers' movement is a negligible small force, compared to the ones discussed earlier (Cuffey and Paterson, 2010).

The actual ice flow velocity depends on the effectiveness of resisting forces counteracting the sum of driving stresses.
The vertical velocity profile is of high interest when it comes to ice core dating and analysis. Ice cores are typically drilled on the ice divide. In that way, it can be assumed that horizontal displacement is negligibly small. To get a handle on the vertical velocities, a dependency between horizontal surface velocities and accumulation rates has been established, which will be presented later on in chapter 3.

## 2.4 Cold as ice - but how cold is that?

The temperature distribution within an ice mass as well as the mean temperature can vary considerably, depending on the location of the glacier. A terminology has been established that groups glaciers in three categories.

- *cold glaciers*: The ice is below melting point throughout the whole glacier or only the glacier bed reaches melting point temperatures.
- *polythermal glaciers*: An ice layer near bedrock is at melting point temperatures.
- *temperate glaciers*: The ice is at melting point throughout the whole glacier except a surface layer of about 15 m, that shows seasonally fluctuating temperatures.

However in reality, one glacier can also show more than one categorical behaviour in different sections. In general, ice is an effective thermal insulator, reacting slowly to environmental temperature changes. Therefore seasonal temperature signals can only be observed down to a depth of 20 m below surface. The annual surface mean temperature can be estimated by measuring the ice temperature at ten to 15 m below surface as long as summer melt is minor (Cuffey and Paterson, 2010).

### 2.4.1 Heat transfer in ice sheets

Ice temperatures within an ice sheet are a result of heat conduction and advection and in some cases melting and refreezing of water constitutes as well (Cuffey and Paterson, 2010). Conduction takes place in vertical and horizontal directions, however the latter might be insignificant due to small temperature gradients in horizontal directions. An ice parcel at a specific location will experience a temperature change according to the basic differential equation of heat conduction with $z$ being the height above bedrock in meter.

$$\frac{\delta T}{\delta t} = \kappa \frac{\delta^2 T}{\delta z^2} - w(z)\frac{\delta T}{\delta z} - u(x)\frac{\delta T}{\delta x} \tag{2.1}$$

The first term describes the conduction with $\kappa$ being the diffusivity of ice in $m^2$/year, which is dependent on the thermal conductivity $K$ [W/mK] of ice, the density $\rho$ and the thermal specific capacity $c$ of ice [J/kgK] in the way: $\kappa = K/(\rho c)$. Density below

the firn layer is assumed to be constant at the density of ice $\rho_{ice} = 917\,\mathrm{kg/m^3}$. $c$ and $K$ are temperature dependent.

$$K_{ice} = 9.828e^{-0.0057T} \tag{2.2}$$

$$c = 152.5 + 7.122T \tag{2.3}$$

with temperature $T$ in Kelvin. The relations are found empirically and taken from Cuffey and Paterson (2010). The second right hand term in equation 2.1 is the vertical advection term being significantly more important than the third term, the horizontal advection of heat. The latter term is often neglected, due to low horizontal temperature gradients.
This formula is valid for the bigger part of the ice sheet. However, as discussed in section 2.2 the firn section has densities smaller than $\rho_{ice}$. The thermal conductivity $K$ depends on the contact area i.e. packing stage of ice crystals, and hence the thermal diffusivity $\kappa$ is dependent on density, whereas the thermal capacity is unaffected by the densification stage. Weller and Schwerdtfeger (1970) describe the dependency with:

$$K(T, \rho) = K_{ice}\left(\frac{\rho(z)}{\rho_{ice}}\right)^{1-\frac{\rho(z)}{2\rho_{ice}}} \tag{2.4}$$

implying

$$\kappa(T, \rho) = \frac{K_{ice}}{c\rho_{ice}}\left(\frac{\rho(z)}{\rho_{ice}}\right)^{1-\frac{\rho(z)}{2\rho_{ice}}} \tag{2.5}$$

To account for that, equation 2.1 is extended with a compaction term and should now allow for density and temperature dependencies of the thermal parameters. Johnsen (1977) therefore introduced the formula:

$$\frac{\delta T}{\delta t} = \kappa \frac{\delta^2 T}{\delta z^2} + \left( \left( \frac{\kappa}{\rho} + \frac{\delta \kappa}{\delta \rho} \right) \frac{\delta \rho}{\delta z} - w(z) \right) \frac{\delta T}{\delta z} + \left( \frac{\delta \kappa}{\delta T} + \frac{\kappa}{c} \frac{\mathrm{d}c}{\mathrm{d}T} \right) \left( \frac{\delta T}{\delta z} \right)^2 - u(x) \frac{\delta T}{\delta x} + L \frac{\Lambda g}{c \rho^3} \frac{\mathrm{d}\rho}{\mathrm{d}z} \quad (2.6)$$

where,

| | | |
|---|---|---|
| $T$ | = Temperature | [°C] |
| $t$ | = time | [year] |
| $z$ | = height above bedrock | [m] |
| $x$ | = horizontal distance from the vertical | [m] |
| $\kappa$ | = thermal diffusivity of firn or ice dependent on $T$ and $\rho$ | [$m^2$/year] |
| $\rho$ | = density at $z$ | [kg/$m^3$] |
| $w(z)$ | = vertical velocity | [m/year] |
| $u(x)$ | = horizontal velocity | [m/year] |
| $c$ | = specific heat capacity of ice | [J/(kg°C)] |
| $L$ | = overlying load at $z$ | [kg/$m^2$] |
| $\Lambda$ | = annual rate of accumulation | [kg/(m year)] |
| $g$ | = acceleration of gravity | [m/$s^2$] |

This formula does not take refreezing of meltwater into account. Snow melted during warmer summer months percolates down through the firn and refreezes at a depth, where temperatures stay below melting point. This refreezing sets free thermal energy, which heats the surrounding ice and may erase former cold winter temperature signals. In areas with high melting rates during summer this should be taken into account.

### 2.4.2 Borehole temperature profile as proxy

When snow falls onto an ice sheet, it remembers the surrounding surface temperature and carries that signal as it sinks into the ice mass. Hence it is possible to make assumptions about past temperature histories when analysing the temperatures measured in an ice core borehole. As vertical flow is considerably slow, the upper part of a vertical temperature profile carries information about recent temperature variations such as seasonal signals, whereas the profile at mid-depths contains information about temperature records of centenial to millenial time scales. Temperatures measured near bedrock, are affected by the *geothermal heat flux*, warming the ice sheet from below. Depending on the overall length of the borehole, temperature signals in the middle parts could have also faded. In a short ice core, only the temperature signals in the top are relatively undisturbed by the geothermal heat. This

heat originates from the primordial energy stored in the heat of the inner core of the Earth, as well as energy that is set free when radioactive elements in the lithosphere decay. The magnitude of this geothermal heat flux varies locally due to earth crust thickness variations and plate tectonics. In Greenland, a geothermal heat flux of $\sim$50 mW/m$^2$ has been calculated from borehole temperature gradients near bedrock (Vinther et al., 2009b). Therefore, against common assumptions, the ice at bedrock will most likely be the warmest part of the ice slab. Depending on the overall climatic regime, it will simultaneously be warmed or cooled from the surface. It takes up to ice-age cycle timescales ($\sim$ 100,000 years) to erase cold glacial temperature "records" within the ice sheet, depending on its height. Nowadays, a *cold spot* can be seen in most of the borehole temperature profiles currently available. It is the remnant of the cold temperatures during the last glacial. When analysing temperature borehole profiles to make assumptions about paleotemperatures of glacials and interglacials, it is necessary to consider changing accumulation rates through time.

### 2.4.3 $\delta^{18}$O as proxy

A water molecule consists of two hydrogen as well as one oxygen molecule. The oxygen atom on earth is present in three stable isotopologe-forms: The light and abundant $^{16}$O-isotopologue and the heavier and rare $^{18}$O-isotopologue. The third species, $^{17}$O, is very rare and not discussed in this thesis. Likewise, there are two hydrogen atom species : An abundant light $^{1}$H-version and a rare, heavier $^{2}$H-isotopologue (also called Deuterium D). The combination of the atoms then yields three common water species:

$$H_2^{16}O : HD^{16}O : H_2^{18}O$$

With a ratio of appearance in nature in the order from above (Dansgaard, 1964):

$$997680 : 320 : 2000\,ppm$$

The used nomenclature calls the two rarer versions by their heavier isotope, hence they are referred to as D and $^{18}$O, whereas $H_2^{16}O$ is called the light or common species. The chemical characteristics of all are similar since they contain an equal number of electrons and protons and only differ in their neutron-number. The position of the heavy atom, causes the vibrational and rotational energies to be different for each species. This explains why the different water species have different vapor pressures. They all behave like water and go through phase changes. However, a light molecule will evaporate more easily from a batch of water molecules, since less energy is needed to evaporate it compared to a heavy molecule. That energy is taken from the surrounding, which links the ambient temperature to the likelihood of "heavy water" evaporation. The opposite is the case in condensation. Here, the heavy molecules tend to easier transform into liquid phase compared to the lighter

version when temperatures drop.
Consequently, the amount of heavy water molecules, taken up by a dry air parcel, depends on the surrounding temperature. When this air parcel cools down, it will get more depleted in its $^{18}$O content, since the heavy molecules are the first ones to be rained out. This implies, the colder the prevailing conditions, the more negative the $\delta^{18}$O value will be of the remaining water in gas phase. This schemata is shown in Figure 2.3. The term *fractionation* is used when talking about the ratio how likely it is, that one heavy species will change phase in regard to the light species. The rare-abundant water molecule ratio is commonly stated as relative deviation from a standard (**S**tandard **M**ean **O**cean **W**ater (**SMOW**)) and due to very small numbers, the value is typically given in per mil. The corresponding formula is:

$$\delta^{18}O = \left( \frac{\frac{H_2^{18}O}{H_2^{16}O}_{sample}}{\frac{H_2^{18}O}{H_2^{16}O}_{SMOW}} - 1 \right) \cdot 1000‰ \tag{2.7}$$

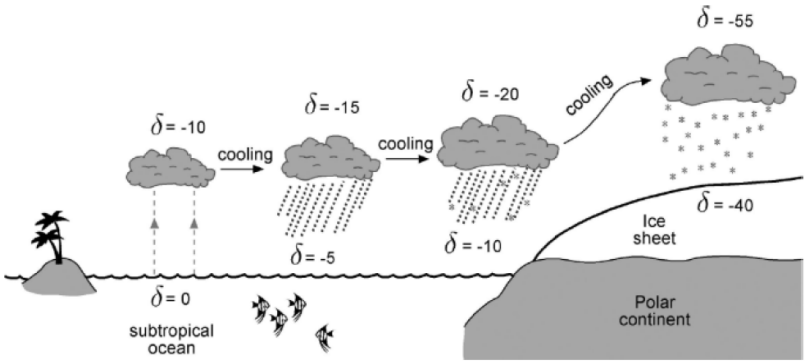


FIGURE 2.3: **Idealised concept of fractionation along the first half of the water cycle**
The uptake of water in warm equatorial areas and the transport towards the pole caps is depicted. Values for the ongoing depletion in $\delta^{18}$O of the water vapor are given as an example (Cuffey and Paterson, 2010).

The dominant evaporation areas on earth are the equator regions. Here a lot of sunlight energy is present to enable evaporation. The air, containing water vapour, is then transported polewards and will continuously cool down. When the saturation deficit is reached, parts of the water vapour will condensate and precipitate whereas the remaining water molecules are transported further until eventual condensation/freezing. Precipitation in form of snow will preserve the isotope and therefore temperature signal in a snow layer, which might turn into ice making the signal available until the ice melts or the carrying ice layer is thinned down to unrecognizability. It has therefore been discovered, that the relative concentration of $^{18}$O to $^{16}$O in ice is related to the prevailing climatic conditions during the time it was deposited as snow or water (Dansgaard, 1964). This means, that by analyzing

ice samples for water isotope concentrations, conclusions about temperature as well as precipitation can be drawn. The T/$\delta^{18}$O-sensitivity is high enough, to recognize seasonal amplitudes in the firn layer.
Assuming that the $^{18}O/^{16}O$ ratio of the original water is constant over time, the $^{18}O$ concentration in the precipitant can be translated into a temperature signal using an empirical linear relationship (Dansgaard, 1964). The parameters found for this dependency seem to be different for different locations and different time periods on Earth (Jouzel et al., 1997).

# Chapter 3

# Models, Methods and Data

## 3.1 Density model

The process of firn turning into ice is driven by new snow accumulating on top of the old snow and compacting the layers below. Various models have been established to simulate this densification process. The generally accepted basis is the linear relationship between the proportional change in air space and the overburden load of snow. Schytt (1958) expresses this dependency as

$$\frac{\boldsymbol{d}\rho}{\rho_{ice} - \rho(d)} = k\rho\,\boldsymbol{d}d \tag{3.1}$$

with $k$ being the inverse folding depth which needs to be determined and depth $d$. In Schytt's model, one exponential function is used to model the densification in firn by tuning factor $k$. However, when plotting depth against measured densities written as $log\left(\frac{\rho(d)}{\rho_{ice}-\rho(d)}\right)$, it reveals a linear relationship, but with different slopes for different stages of the densification. Therefore, Herron and Langway (1980) have developed a two stage densification model for densities up to close-off densities. The first densification stage is modelled for densities $\rho <= \rho_{crit}$, whereas the second stage then describes densification for $\rho_{crit} <= \rho <= \rho_{co}$ (see section 2.2). They find the best fit for the previously described dependency and rearrange equation 3.1 in a way, that it now contains temperature and accumulation dependencies, that are assumed to be constant for a certain site.

The densification rate is described as:

$$\frac{\mathrm{d}\rho}{\mathrm{d}t} = \begin{cases} K_0\lambda^a(\rho_{ice} - \rho(d)), & \text{for } \rho <= \rho_{crit} \quad (3.2) \\ K_1\lambda^b(\rho_{ice} - \rho(d)), & \text{for } \rho_{crit} <= \rho <= \rho_{co} \quad (3.3) \end{cases}$$

where

$$K_0 = 11exp\left(-\frac{10160}{RT}\right) \quad (3.4)$$

$$K_1 = 575exp\left(-\frac{21400}{RT}\right) \quad (3.5)$$

with

| | | |
|---|---|---|
| $d$ | = depth ..... | [m] |
| $t$ | = time ..... | [years] |
| $\rho(d)$ | = density at depth d | [Mg/m$^3$] |
| $\rho_{ice}$ | = 0.917 (density of ice) ..... | [Mg/m$^3$] |
| $\lambda$ | = accumulation rate in water eq. | [m/year] |
| $a$ & $b$ | = empirical constants ..... | [-] |
| $K_0$ & $K_1$ | = Arrhenius-type rate constants | [] |
| $T$ | = surface temperature ..... | [K] |
| $R$ | = 8.314 (gas constant) ..... | [J/(mol K)] |

It was shown, that the constants $a$ & $b$ can be assumed to have a universal validity for $a = 1$ and $b = 0.5$.
Using the depth-age relationship $\frac{\mathrm{d}d}{\mathrm{d}t} = \frac{\lambda}{\rho}$ equations 3.2 and 3.3 can be rearranged as densifications rates in regard to depth $d$ as:

$$\frac{\mathrm{d}\rho}{\mathrm{d}d} = \begin{cases} K_0(\rho_{ice} - \rho(d))\rho(d) & \text{for } \rho \leq \rho_{crit} \quad (3.6) \\ K_1\lambda^{-0.5}(\rho_{ice} - \rho(d))\rho(d) & \text{for } \rho_{crit} \leq \rho \leq \rho_{co} \quad (3.7) \end{cases}$$

Hence, the first densification stage is independent of the accumulation rate. By integrating equations 3.2, 3.3, 3.6, 3.7 and using a given surface temperature $T$, an accumulation rate $\lambda$ and an initial density $\rho_0$ the density and age of the firn at any depth $d$ can be calculated. Moreover, the $\Delta$-age at close-off depth can be estimated. When assessing the critical depth it becomes obvious that the colder the location, the deeper is the stage transition. The second stage is dependent on accumulation rates and it is shown that more accumulation leads to deeper close-off depths. Consequently, the $\Delta$-age is smaller compared to locations with low accumulation rates.

In this thesis, density measurements from the old and the new core were combined in order to find one universally valid densification model following the Herron-Langway approach. It needs to be mentioned that the quality of the old core was rather low due to dry drilling techniques and data below 100.1 m, when measurements became too scattered, was discarded. Density data for the new core is available to a depth of 100.925 m. The second to last measurement is missing, which

is why this data point was interpolated from the neighboring ones. Originally the Herron-Langway model uses observed values for the initial density. In order to improve the fit in this thesis, the model was allowed to choose the initial and critical density as two additional tuning parameters.

## 3.2 Ice flow model

The fundamental law of any ice flow model is the mass conservation law since no mass is lost nor built up during the flow process. The corresponding equation is the continuity equation:

$$\frac{\delta \rho}{\delta t} + \frac{\delta u}{\delta x} + \frac{\delta v}{\delta y} + \frac{\delta w}{\delta z} = 0 \tag{3.8}$$

with time $t$, velocity components $(u, v, w)$ and the coordinate system orientation $(x, y, z)$. We further assume in-compressible ice and a steady-state ice sheet. Equation 3.8 is then simplified to a dependency between horizontal and vertical velocities.

$$-\frac{\delta u}{\delta x} = \frac{\delta w}{\delta z} \tag{3.9}$$

This relationship can now be used to calculate the vertical velocity with the help of horizontal surface velocities, without knowing the actual surface velocity. This is due to the steady-state assumption, which allows to express the horizontal surface velocity with known site-specific accumulation rates. The early Nye flow model assumed a constant vertical strain-rate from bottom to ice sheet surface (Nye, 1951). However, Willi Dansgaard and Sigfus Johnsen introduced a new model, which assumes unconstrained flow down to a certain depth (Dansgaard and Johnsen, 1969). This model calculates warmer bottom temperatures, which then proved to be closer to the observed ice temperatures.

### 3.2.1 Original Dansgaard-Johnsen model

The ice flow model introduced to model the age and flow for the Camp Century ice core is called the *kink-model*. It assumes unconstrained horizontal flow of ice $u_H$ down to a certain kink depth (or kink height $h$) and linear decreasing with depth until bedrock due to shear forces $u_H(f_B + (1 - f_B)\frac{z}{h})$. In different versions of the model, the flow becomes zero at bedrock or flows with a velocity ratio $f_B$ of surface and bedrock velocity. The bottom sliding ratio $f_b$ is dependent on temperature, bedrock topography and roughness. A sketch of the model can be seen in Figure 3.1.

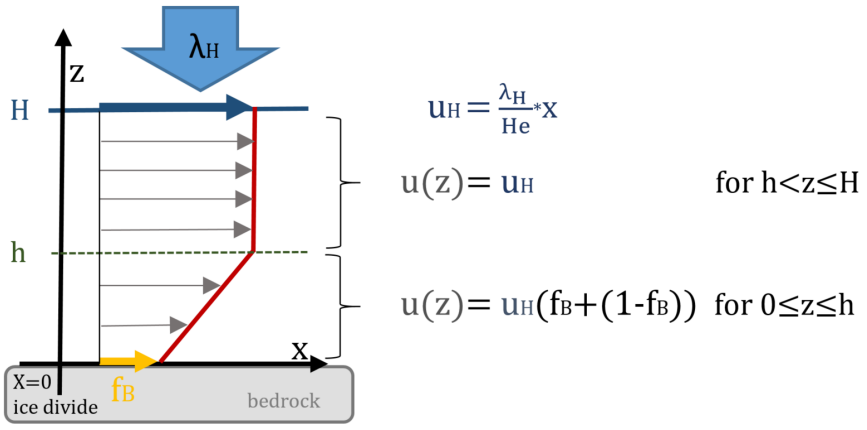


FIGURE 3.1: ***ink-model* scheme**
The qualitative sketch of the horizontal flow regime assuming a *kink-model*. $h$ resembles the kink height (kink depth).

The surface velocity $u_H$ is described with help of the accumulation rate $\lambda_H$. New snow, piling up on the ice sheet thickness $H$ has to be transported away to satisfy the steady-state condition of the ice sheet. The corresponding equations are:

$$\lambda_H * x = \int_0^H u(z)dz$$
$$\lambda_H * x = \int_0^h u_H(f_B + (1-f_B)\frac{z}{h})dz + \int_h^H u_H dz$$
$$\lambda_H * x = u_H(f_B h + \frac{1}{2}(1-f_B)h + (H-h))$$
$$\text{hence}, u_H = \frac{\lambda_H}{He} * x$$
$$\text{with } He = H + \frac{h}{2}(f_B - 1)$$

$He$ is the effective height. It is the theoretical height of the ice sheet, if the ice flow was constant over the whole ice sheet thickness (Figure 3.2). The annual layer thickness at the surface is the same as the accumulation rate $\lambda_H$ and its negative is the vertical velocity ($w$) of the ice at $H$. Hence, equation 3.9 can now be used to formulate vertical velocity and simultaneously annual layer thickness equations.

$$-\frac{\delta u}{\delta x} = \frac{\delta w}{\delta z} = -\frac{\delta \lambda}{\delta z} \tag{3.10}$$
$$\int_{w(z_1)}^{w(z_2)} \mathrm{d}w = -\int_{z_1}^{z_2} \frac{du}{dx}dz' \tag{3.11}$$

where $z$ is height above bedrock.
To solve this integral two cases have to be distinguished. The upper case for heights between kink height and ice sheet surface ($h < z < H$) and the lower case below the kink height ($0 < z < h$). If no melting at bedrock is assumed, the boundary conditions equal $w(0) = 0$ and $w(H) = -\lambda_H$.

Solving the integrals gives vertical velocity and annual layer equations as functions of $z$. Schematically visualised the equations yield a 'height above bedrock-annual layer thickness' plot as can be seen in Figure 3.2. Extending the linear upper part of the graph, the line intersects the y-axis at $0.5 \cdot h$.

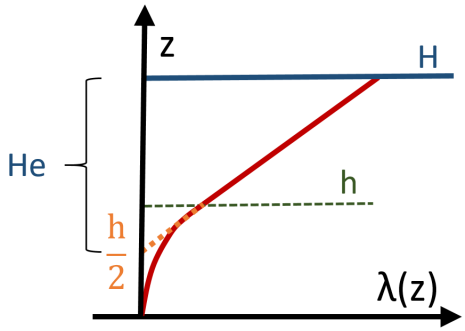


FIGURE 3.2: **Annual layer thickness scheme**
A qualitative diagram of the annual layer thicknesses with depth/height above bedrock. $He$ is the effective height of the ice sheet. The vertical velocity curve looks alike.

### Age calculations

With the vertical velocities calculated for each depth, an age calculation can be performed using again the continuity equation. This age profile can be tested against layer counting or well established age horizons in order to approve the set up flow model. For calculating the age scale the definition of velocity is used:

$$w = \frac{dz}{dt} \tag{3.12}$$

$$dt = \frac{dz}{w(z)} \tag{3.13}$$

$$\rightarrow \int_{t(z_1)}^{t(z_2)} dt = \int_{z_1}^{z_2} \frac{1}{w(z)} dz' \tag{3.14}$$

Since the vertical velocity equations are different for above and below the kink height, the age equations must be as well.

## 3.2.2 Modified Dansgaard-Johnsen model

When using the *kink-model* for the two Renland cores, the calculated age does not fit well with the observed horizons. Therefore, a new flow model was developed for the Renland Ice Cap which is presented in this thesis. It is a modification of the *kink-model* which will subsequently be called the *step-model*. Instead of gradual decreasing of the horizontal velocity below the kink height, this model assumes a jump to another constant velocity below *step height* $h$. In reality, the transition from one flow regime to the other will be rather gradual. However, the abrupt transition is chosen

for model-simplicity and model-parameter reduction. The ratio of surface velocity and velocity near bedrock is defined by $f_B$, the step ratio. A schematic drawing of the horizontal flow regime can be seen in Figure 3.3. The scheme includes a layer of ice, frozen to bedrock which is called dead ice. This approach is motivated by the

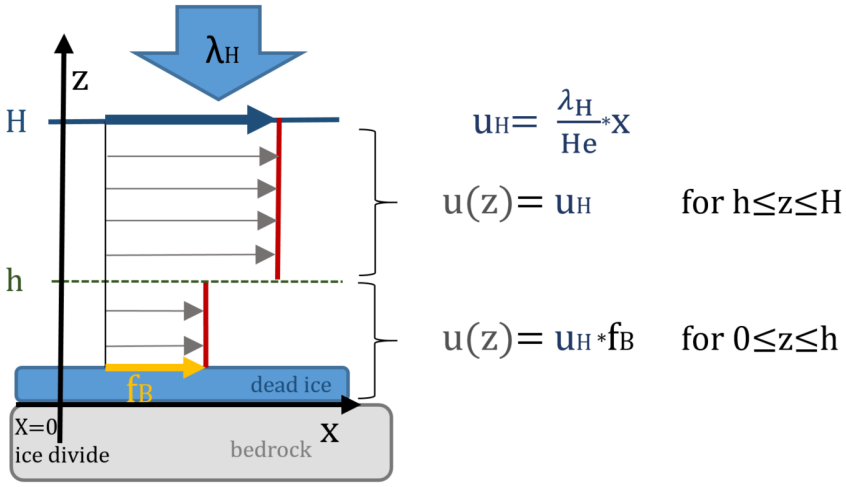


FIGURE 3.3: ***Step-model* scheme**
A qualitative diagram of the horizontal ice flow near the ice divide. $h$ is the step height (or step depth).

Renland bedrock topography. As can be seen in a bedrock surface topography plot in Figure 1.3 the core was drilled in a valley. With the *step-model* an unconstrained flow of ice is assumed above the mountain ridge whereas the flow is constrained by the mountains within the valley. The equations used for calculating vertical velocity and age have the same format as the equations introduced for the *kink-model* earlier. The horizontal velocity $u(z)$ equations are:

$$u(z) = \begin{cases} u_H & \text{for } h \leq z \leq H \\ u_H * f_B & \text{for } 0 < z \leq h \end{cases}$$

Where $z$ is height above bedrock, $H$ is total height of ice sheet and $h$ is the step height.

$u_H$ derived from steady-state assumption and as a function of $\lambda_H$:

$$\lambda_H * x = \int_0^H u(z)dz$$
$$\lambda_H * x = \int_0^h f_B * u_H dz + \int_h^H u_H dz$$
$$\lambda_H * x = f_B * u_H * h + u_H * H - u_H * h = u_H * (H - h * (1 - f_B))$$
$$\text{hence, } u_H = \frac{\lambda_H}{He} * x$$
$$\text{with, } He = H - h * (1 - f_B)$$

Again the continuity equation allows to formulate vertical velocities:

$$-\frac{du}{dx} = \frac{dw}{dz}$$
$$\int_{w(z_1)}^{w(z_2)} dw = -\int_{(z_1)}^{(z_2)} \frac{du}{dx} dz'$$

The boundary conditions are the same as mentioned above. Splitting the integral in two parts the equations reveal:
For $0 < z \leq h$**:**

$$\int_{w(0)}^{w(z)} dw = -\int_0^z \left(\frac{f_B \lambda_H}{He}\right) dz'$$
$$w(z) = w(0) - \left[\frac{f_B \lambda_H}{He} * z'\right]_0^z$$
$$w(z) = \frac{-f_B \lambda_H}{He} * z$$

For $h \leq z \leq H$**:**

$$\int_{w(z)}^{w(H)} dw = -\int_z^H \left(\frac{\lambda_H}{He}\right) dz'$$
$$w(z) = w(H) + \left[\frac{\lambda_H}{He} z'\right]_z^H$$
$$w(z) = -\lambda_H + \frac{\lambda_H}{He} H - \frac{\lambda_H}{He} z$$
$$w(z) = -\frac{\lambda_H}{He}(He - H + z)$$
$$w(z) = -\frac{\lambda_H}{He}(z - h(1 - f_B))$$

Taking the vertical velocities equations, the equations for age as function of height above bedrock can be derived:

$$w(z) = \frac{dz}{dt}$$
$$dt = \frac{dz}{w(z)}$$
$$\rightarrow \int_{t(z_1)}^{t(z_2)} dt = \int_{z_1}^{z_2} \frac{1}{w(z)} dz'$$

The boundary condition $t(H) = 0$ is known. Therefore, the equations for the age of the ice are:

For $h \leq z \leq H$**:**

$$
\begin{aligned}
w(z) &= -\frac{\lambda_H}{He}(z - h(1 - f_B)) \\
\int_{t(z)}^{t(H)} dt &= \int_z^H \frac{1}{-\frac{\lambda_H}{He}(z - h(1 - f_B))} dz' \\
\int_{t(H)}^{t(z)} dt &= -\frac{He}{\lambda_H} \int_H^z \frac{1}{(z - h(1 - f_B))} dz' \\
t(z) &= t(H) - \frac{He}{\lambda_H} ln[z' - h(1 - f_B)]_H^z \\
t(z) &= -\frac{He}{\lambda_H}(ln(z - h(1 - f_B)) - ln(H - h(1 - f_B))) \\
t(z) &= \frac{He}{\lambda_H} ln\left(\frac{He}{z - h(1 - f_B)}\right)
\end{aligned}
$$

Hence, the age of the ice at the step height is known:

$$
\begin{aligned}
t(h) &= \frac{He}{\lambda_H} ln\left(\frac{He}{h - h(1 - f_B)}\right) \\
t(h) &= \frac{He}{\lambda_H} ln\left(\frac{He}{f_B * h}\right)
\end{aligned}
$$

This can be used to calculate the equations for $0 < z \leq h$**:**

$$
\begin{aligned}
w(z) &= \frac{-f_B \lambda_H}{He} z \\
\int_{t(z)}^{t(h)} dt &= \int_z^h \left(\frac{1}{\frac{-\lambda_H f_B}{He} z}\right) dz' \\
t(z) &= t(h) + \frac{He}{f_B \lambda_H} ln[z']_z^h \\
t(z) &= t(h) + \frac{He}{f_B \lambda_H} ln\left[\frac{h}{z}\right]
\end{aligned}
$$

### 3.2.3 Used age markers

Both ice cores were matched to the GICC05 timescale in order to be comparable. This study focuses on modelling the ice flow and temperatures within the Holocene period (11,700 b2k - today). Throughout this period accumulation rates are assumed to be constant. Therefore available age markers down to a depth of 532 m were used when modelling the ice flow at the RECAP site. For the Renland site, age fixpoints down to 280 m were used for the ice flow model. Below, observed annual layers increase in thickness, i.e. layer thinning stopped.

## 3.3 Borehole temperature model (BTM)

In order to model borehole temperatures at the Renland Ice Cap, a coupled heat-and ice flow model including a densification model for the firn layer is used. Additionally, upper boundary and lower boundary conditions have to be defined. Upper boundary conditions are given by a surface temperature forcing and lower boundary conditions are defined by the geothermal heat flux from the bedrock. The non-steady state heat conduction (equation 2.6) is used to describe the temperature profile behaviour. However, being close to the ice divide, horizontal ice flow and the comparably small horizontal temperature gradient is neglected. To solve this equation for the temperature at all depths at any given point in time, the numerical method of Crank-Nicolson is used (Crank and Nicolson, 1996),

### 3.3.1 Non-steady state numerical model

In this paragraph, the Crank-Nicolson method is explained by starting out with the simple heat equation 2.1 and extending it for the whole heat equation 2.6 after the basic principle is described.

Consider the basic heat conduction formula which was introduced in section 2.4.1:

$$\frac{\delta T}{\delta t} = \kappa \frac{\delta^2 T}{\delta z^2} - w(z) \frac{\delta T}{\delta z} \tag{2.1}$$

For it to be solved numerically, it needs to be re-written in discrete form concerning time ($t$) and location within the ice sheet ($z$). The calculations are done for time steps ($\Delta t$) and height steps ($\Delta z$) which are referred to with $i$- and $j$-indices respectively. 2.1 can then be written as:

$$\begin{aligned} \frac{T_{i+1,j} - T_{i,j}}{\Delta t} =& \frac{\kappa}{2} \left( \frac{T_{i+1,j+1} - 2T_{i+1,j} + T_{i+1,j-1}}{\Delta z^2} + \frac{T_{i,j+1} - 2T_{i,j} + T_{i,j-1}}{\Delta z^2} \right) \\ & - \frac{w(z)}{2} \left( \frac{T_{i+1,j+1} - T_{i+1,j-1}}{2\Delta z} + \frac{T_{i,j+1} - T_{i,j-1}}{2\Delta z} \right) \end{aligned}$$

Re-arranging in a way, that everything except the temperature terms are outside the parenthesis gives:

$$\begin{aligned} T_{i+1,j} - T_{i,j} =& \frac{\kappa \Delta t}{2\Delta z^2} \left( T_{i+1,j+1} - 2T_{i+1,j} + T_{i+1,j-1} + T_{i,j+1} - 2T_{i,j} + T_{i,j-1} \right) \\ & - \frac{w(z)\Delta t}{4\Delta z} \left( T_{i+1,j+1} - T_{i+1,j-1} + T_{i,j+1} - T_{i,j-1} \right) \end{aligned}$$

All unknown "next time step"-terms ($i+1$) are now sorted to the left side, whereas all known terms of the current time step ($i$) are to the right of the equal sign. This equation is valid for the whole borehole, i.e. $j_n$. Additionally the diffusion and

convection terms in front of the parenthesis are substituted for

$$\text{Diffusion: } s_j = \frac{\kappa \Delta t}{2\Delta z^2}$$
$$\text{Convection: } r_j = \frac{w(z)\Delta t}{4\Delta z}$$

Hence it now reads:

$$(r_j - s_j)T_{i+1,j+1} + (1 + 2s_j)T_{i+1,j} + (-r_j - s_j)T_{i+1,j-1} \\ = (s_j - r_j)T_{i,j+1} + (1 - 2s_j)T_{i,j} + (s_j + r_j)T_{i,j-1} \quad (3.15)$$

Since it is desired to include a firn layer and use equation 2.6 instead of 2.1, the convection term $r_j$ needs to account for temperature as well as density dependencies of the thermal parameters $c$ and $\kappa$ and a compaction term needs to be introduced. The terms of equation 2.6 that needs to be incorporated in term $r_j$ are the following:

$$\text{a)} \left( \left( \frac{\kappa}{\rho} + \frac{\delta \kappa}{\delta \rho} \right) \frac{\delta \rho}{\delta z} - w(z) \right) \frac{\delta T}{\delta z}$$
$$\text{b)} \left( \frac{\delta \kappa}{\delta T} + \frac{\kappa}{c} \frac{\mathrm{d}c}{\mathrm{d}T} \right) \left( \frac{\delta T}{\delta z} \right)^2$$

First, the b)-term needs to be linearised, i.e. one derivation has to be re-written in discrete form. This is done using the forward *Euler-scheme* and substituting it for $D$ (Kalnay, 2003).

$$\left( \frac{\delta T}{\delta z} \right)^2 = \left( \frac{\delta T}{\delta z} \right) \left( \frac{T_{i,j+1} - T_{i,j}}{\Delta z} \right) = \left( \frac{\delta T}{\delta z} \right) D$$

a) and b) can now be written in one term, which is influencing the vertical temperature advection term.

$$\left( \left( \frac{\kappa}{\rho} + \frac{\delta \kappa}{\delta \rho} \right) \frac{\delta \rho}{\delta z} - w(z) + \left( \frac{\delta \kappa}{\delta T} + \frac{\kappa}{c} \frac{\mathrm{d}c}{\mathrm{d}T} \right) D \right) \left( \frac{\delta T}{\delta z} \right) \quad (3.16)$$

The b) term above contains two derivations of thermal capacity and diffusivity for temperature. Those can be calculated from equations 2.3 and 2.5 respectively.

$$\begin{aligned}
\frac{\mathrm{d}c}{\mathrm{d}T} &= 7.122 \\
\frac{\delta\kappa}{\delta T} &= \frac{\delta}{\delta T}\left(K_{ice}(T)\frac{1}{c(T)}\right)P \\
&= \left(\frac{\delta K_{ice}}{\delta T}\frac{1}{c} + \frac{\delta c^{-1}}{\delta T}K_{ice}\right)P \\
&= \left(-0.0057\frac{K_{ice}}{c} - 7.122\frac{K_{ice}}{c^2}\right)P \\
&= -0.0057\kappa - 7.122\frac{\kappa}{c} \\
\text{with } P &= \frac{1}{\rho_{ice}}\left(\frac{\rho(z)}{\rho_{ice}}\right)^{1-\frac{\rho(z)}{2\rho_{ice}}}
\end{aligned}$$

Note that the dependency of density on temperature is neglected in the derivation. This is due to the borehole temperature model set-up, which uses one density model throughout the whole model time-frame. I.e. it is assumed that recent annual mean temperatures as well as accumulation rates are representative for the Holocene period, which is modelled in this thesis. Term b) can now be written in a simple form

$$\begin{aligned}
\left(\left(\frac{\delta\kappa}{\delta T} + \frac{\kappa}{c}\frac{\mathrm{d}c}{\mathrm{d}T}\right)D\right)\left(\frac{\delta T}{\delta z}\right) &= \left(\left(-0.0057\kappa - 7.122\frac{\kappa}{c} + \frac{\kappa}{c}7.122\right)D\right)\left(\frac{\delta T}{\delta z}\right) \\
&= -0.0057\kappa D\left(\frac{\delta T}{\delta z}\right)
\end{aligned}$$

As a next step, the derivatives for the density dependency of the thermal diffusivity, as well as the density derivative for depth in term a) need to be calculated. Again, equation 2.5 is used for the diffusivity derivation.

$$\frac{\delta\kappa}{\delta\rho} = \kappa\left(\frac{1}{\rho(z)} - \frac{1}{2\rho_{ice}}\right)\left(1 + log\left(\frac{\rho(z)}{\rho_{ice}}\right)\right)$$

Since the density model is a two *step-model*, the derivation for depth is as well. The equations are the same as 3.6 and 3.7.

$$\frac{\delta\rho}{\delta z} = \begin{cases} \text{equation 3.6} & \text{for } \rho \leq \rho_{crit} \\ \text{equation 3.7} & \text{for } \rho_{crit} \leq \rho \leq \rho_{co} \end{cases}$$

The convection term $r_j$ now sums up to:

$$r_j = \left(w(z) + 0.0057\kappa D - \left(\frac{\kappa}{\rho} + \frac{\delta\kappa}{\delta\rho}\right)\frac{\delta\rho}{\delta z}\right)\frac{\Delta t}{4\Delta z}$$

Equation 3.15 is re-arranged in vector-notation in a way, that the right hand side

still consists of the "known"-elements ($f_n$), whereas the left hand side formulates the equations for the unknown-elements ($i+1$).

$$\begin{bmatrix} b_1 & c_1 & 0 & \cdots & 0 \\ a_2 & b_2 & c_2 & \ddots & \vdots \\ 0 & a_3 & b_3 & \ddots & \vdots \\ \vdots & \ddots & \ddots & \ddots & c_{n-1} \\ 0 & \cdots & \cdots & a_n & b_n \end{bmatrix} \begin{bmatrix} T_{i+1,1} \\ T_{i+1,2} \\ T_{i+1,3} \\ \vdots \\ T_{i+1,n} \end{bmatrix} = \begin{bmatrix} f_1 \\ f_2 \\ f_3 \\ \vdots \\ f_n \end{bmatrix} \tag{3.17}$$

The positive orientation of the model is from bedrock to ice sheet surface. The $f_n$ vector expresses the known temperature at time step $i$ and is the weighted sum of the surrounding temperatures from the previous times step $i-1$. For all non-boundary spatial-conditions $1 < j < n$, $f$ comprises of everything that is on the right hand side of equation 3.15 plus the last term of equation 2.6, the compaction term:

$$f_j = (s_j - r_j)T_{i,j+1} + (1-2s_j)T_{i+1,j} + (s_j + r_j)T_{i,j-1} + L\frac{\Lambda g}{\rho^3 c}\frac{\mathrm{d}\rho}{\mathrm{d}z}$$

The three diagonals $a_j$, $b_j$ and $c_j$ comprise the diffusion and convection terms $s_j$ and $r_j$ and define the boundary conditions of the model. They represent the spatial segmentation with $a_j$ being the previous $j-1$ segment, $b_j$ being the current position $j$ and $c_j$ expressing the following segment $j+1$. Therefore, for all non-boundary spatial-conditions $1 < j < n$ it is:

$$a_j = -r_j - s_j, \qquad b_j = 1 + 2s_j, \qquad c_j = r_j - s_j$$

The upper boundary condition $j = n$ is the surface temperature, that drives the heat conduction from above. Hence:

$$a_n = 0, \qquad b_n = 1, \qquad c_n = \text{not in matrix}, \qquad f_n = T(H)$$

The lower boundary condition $j = 1$ is given as a temperature gradient at bedrock, which is described with the geothermal heat flux $G_{geo}$ divided by the thermal conductivity $K_{ice}(T)$ multiplied with the spatial increment. This translates to:

$$a_1 = \text{not in matrix}, \qquad b_1 = -1, \qquad c_1 = 1, \qquad f_1 = \frac{Q_{geo}}{K_{ice}(T)}\Delta z$$

As our model runs forward in time, the aim is to calculate temperatures for all spatial segments $n$ for the next time step $i+1$, which is the $T$-vector on the left side of the equal sign in equation 3.17. The vector $T_{i+1,n}$ is calculated by inversion:

$$\mathbf{M}T = f \qquad \rightarrow \qquad T = \mathbf{M}^{\mathrm{T}} f \tag{3.18}$$

For every time step $i$ the previously calculated $T$-vector is used as input vector for $f$ to find the next $T$-vector.

The starting condition is an isothermal temperature profile throughout the whole ice sheet. In the spin up phase of the model run, the model is continuously driven with constant surface temperature as well as constant geothermal heat flux until a steady state temperature profile has evolved. The geothermal heat flux is adjusted in a way, that the steady-state profile matches the three deepest measurement points of the two boreholes respectively. The best fit is found with the least-square technique. From there, various surface temperature forcing scenarios are tested in order to model a BTC which is in good agreement with the observed one.

## 3.4 Comparison of surface temperature forcing

A surface temperature forcing is needed for the BTM. Ideally, a long term Renland weather recording data set would be used. Since such temperature history does not exist, various surface forcing data sets are applied and compared against each other in order to find a reasonable temperature history for Renland. The different temperature scenarios comprise of two different weather stations north and south of Renland, one weather station close to the peninsula and two different regional climate models. The input data is tuned to get the best match between observed and modelled borehole temperatures. In order to quantify the model error, a misfit is calculated for each model run using the following formula:

$$misfit = \frac{\sqrt{\sum_{i=1}^{N}(T_{calc} - T_{obs})^2}}{N} \tag{3.19}$$

$N$ is the number of measurement points and it is used to make the misfit comparable between the two drill sites. Despite the irregular distribution of temperature measurements in the borehole, the error estimation of the temperature borehole fit throughout the thesis was performed using equation 3.19. This is justified with the assumption, that the temperature signal is better preserved in the upper part of the borehole (with more measurements), whereas the signal has smoothed out/diffused significantly in the lower part. Moreover, temperature records of several decades are used for the surface forcing. Those will only travel down halfway through the ice cap which makes it reasonable to place the emphasis on fitting the upper measurement points.
In the following, the different surface forcing scenarios are presented.

### 3.4.1 DMI - weather stations

The Danish Meteorological Institute runs various automatic weather observation stations scattered around Greenland's coast. The three weather stations mentioned in this thesis are presented in Table 3.1. The closest one to the Renland peninsula is Ittoqqortoormiit, which can be seen in Figure 1.1. The datasets used are the ones

TABLE 3.1: DMI weather stations

| | **number** | **latitude** °N | **longitude** °W | **elevation** m | **recording since** year |
|---|---|---|---|---|---|
| Danmarkshavn | 04320 | 76.7697 | 18.6675 | 11 | 1949 |
| Ittoqqortoormiit | 04339 | 70.4844 | 21.9511 | 70 | 1950 |
| Tasiilaq | 04360 | 65.6167 | 37.6367 | 54 | 1895 |

published by DMI (Cappelen, 2017). Missing data was interpolated between the previous and the following month for single monthly data missing. If data for two consecutive months or more was missing, the values were found by interpolating between the same month of the previous and following year.

#### Temperature data comparison

Ittoqqortoormiit is located at the entrance of the Scoresbysund Fjord. Since the Renland peninsula is almost surrounded by the branches of that fjord, it can be estimated that the climate at both locations is similar. The fjord allows marine climate temperatures to reach inland. However, the elevation difference of over 2000 m is non-negligible and demands for elevation correction of the temperature record.
The coastal Tasiilaq weather station is located 600 km further south. Temperatures are expected to be significantly warmer and less extreme than the Renland climate. A third weather station, Danmarkshavn, 600 km north of Renland is used for comparative analysis of latitudinal effects.

In Figure 3.4, the differences between the three stations is visualised with monthly mean air temperatures of the years 2012-2015. Throughout this thesis, time is running in positive x-axis direction. As can be seen, the three weather station recorded

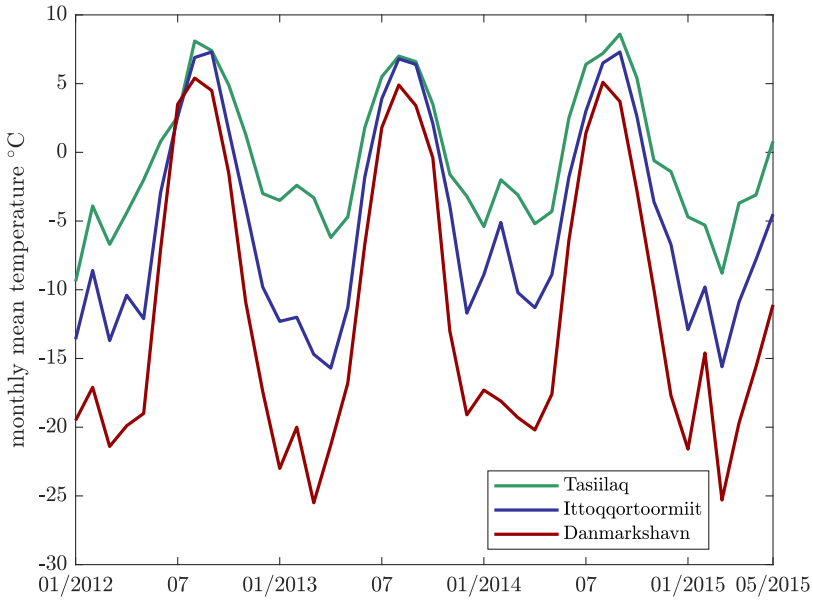


FIGURE 3.4: **DMI weather station temperature records**
The recorded monthly mean temperatures of the three DMI weather stations Ittoqqortoormiit, Tasiilaq and Danmarkshavn are shown for the time span 01/2012-05/2015.

temperatures that show increasing seasonal signal amplitudes with increasing latitude location. The overall curve pattern is similar with mean offsets between the different curves. The calculated means of monthly mean temperature data in the period 1950-2015 for the three stations are:

Tasiilaq: $-1.0°C$ Ittoqqortoormiit: $-6.7°C$ Danmarkshavn: $-11.8°C$

### 3.4.2 Regional Climate Models (RCM)

Climate models are attempts to simulate climate and weather for a specific region and time. They are built from elements which describe and represent real life processes of the climate system. Those interactions are formulated with equations based on the physical understanding of relevant processes. With this, past climate recordings can be forged and future climate behavior simulated. The basis of all climate models is a General Circulation Model (GCM) that can consist of several climate system components, but needs to comprise of a general atmospheric circulation model in order to model weather patterns. Models describing other climate system components can then be coupled to the atmosphere model.
Since climate processes reach from large scale processes to region specific small scale processes, characteristic features of specific areas are further defined in so called Regional Climate Models. They follow the superordinate laws of the GCM but contain

more detailed descriptions of the area to resolve small scale weather patterns. In this thesis, two regional climate models specifically designed for polar regions are tested for their ability to model the borehole temperature curve when used as surface temperature forcing. This could affirm the quality of their model results.

#### HIRHAM5

The **HIRHAM** model was developed by the Danish Meteorological Institute in collaboration with the Max Plank Institute. Underlying is the coupled ocean-atmosphere circulation model EC**HAM** GCM model that defines the basic physical parameterisation schemes. Additionally, the HIRHAM model includes dynamics described in the **HIR**LAM (High Resolution Limited Area Model) and is thus able to simulate local climate variations of the Greenland area (Christensen et al., 2007). The here used model is the HIRHAM5 GL2 version. Its boundary conditions are defined by re-analysis data of the ERA-Interim data set (Dee et al., 2011). HIRHAM5's resolution is a 5 km horizontal grid and an irregular 31-step vertical resolution determined by pressure intervals. The monthly two meters above surface temperature data has a mean of -19.59°C when calculated for the whole available time series from 1980-2014 in the RECAP grid cell. The ice mask, used in the HIRHAM5 model is the one defined by the Programme for Monitoring of the Greenland Ice Sheet (PROMICE) group at GEUS institute. In Figure 3.5 one can see the ice mask together with the contour lines of the topography of the Arctic digital elevation model (DEM) (PGC, 2017).

#### RACMO2.3

The second RCM used in this study is version 2.3 of the Regional Atmospheric Climate Model (RACMO2.3) which was developed at Utrecht University (Noël et al., 2017). It combines the dynamical core of the High Resolution Limited Area Model (HIRLAM) with the physical dynamics of the CY33r1 package of the European Center for Medium-range Weather Forecasts Integrated Forecast System (ECMWF-IFS). The herein used polar version (p2) of the model incorporates a multi-layer snow element that captures snow-specific processes like melt, refreezing and runoff. It further takes surface albedo processes into account (Utrecht University, 2018). The ice mask of the model has a resolution of 11 km as well as the model outcome. The herein used data was statistically downscaled to 1 km resolution (Noël et al., 2016). The mean of the two meters above surface temperature for the monthly time series 1958-2016 is -14.3°C (RECAP location), and -14.4°C (Renland 1988 location). The same ice mask as used in the HIRHAM model was used in this model and its properties together with the contour lines of the topography of Arctic DEM are shown in Figure 3.5 (PGC, 2017).

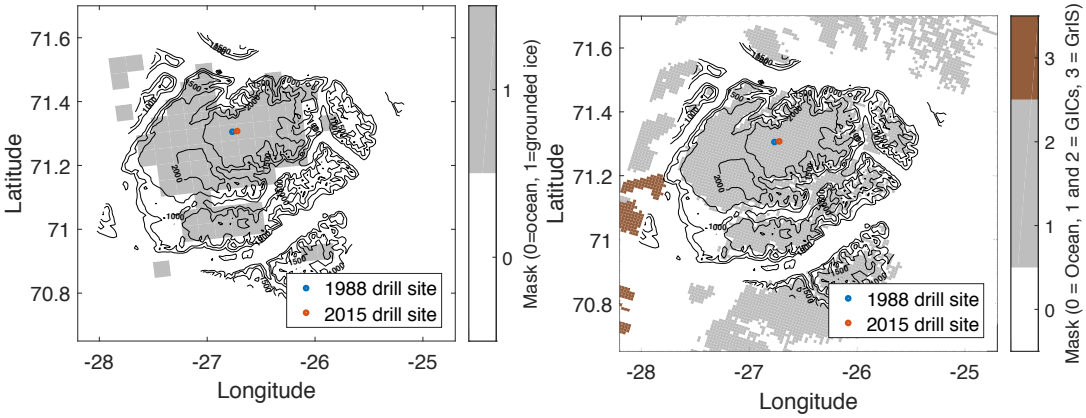


FIGURE 3.5: **Glacier mask of HIRHAM (left) and RACMO (right) model**
The Renland area as well as the two drill site locations are shown in the plots. The gray areas define Greenland ice caps (GICs) and the brown areas the main Greenland ice sheet (GrIS).
(credits: Iben Koldtoft,DMI)

### Performance of RCM for Tasiilaq

The DMI station Tasiilaq is found to have the HIRHAM model coordinates (65.6410°N/-37.6123°E). The calculated mean for the monthly data series is -0.1159°C and the modelled temperature record can be compared against the observed temperature record for the timespan 01/1980-12/2014 in Figure 3.6. The curves seem to be in good agreement and the calculated linear coefficient of determination of $R^2$=0.89 confirms this (P<0.01). The HIRHAM5 model data has a tendency to be warmer than the observations which is confirmed when comparing the mean of all monthly data available. The DMI Tasiilaq station recorded a mean of -1.1 °C whereas the HIRHAM5 model mean for monthly data is roughly one degree warmer. The Tasiilaq position in the RACMO model (65.6181°N/-37.6356°E) is a water grid cell and therefore carries no temperature data. The four closest grid cells with data are combined in a mean of monthly mean data. The positions used are (65.6073°N/-37.7683°E), (65.6172°N/-37.7868°E), (65.6282°N/-37.8266°E), (65.6348°N/-37.7814°E). Like the HIRHAM model, the RACMO model also shows a high correlation with the DMI data of $R^2$=0.95 (P<0.01). However, RACMO has the tendency to be colder than the observed data. The mean of the temperature data series used for the plot above is -2.99 °C which is about two degrees colder than the recorded mean.

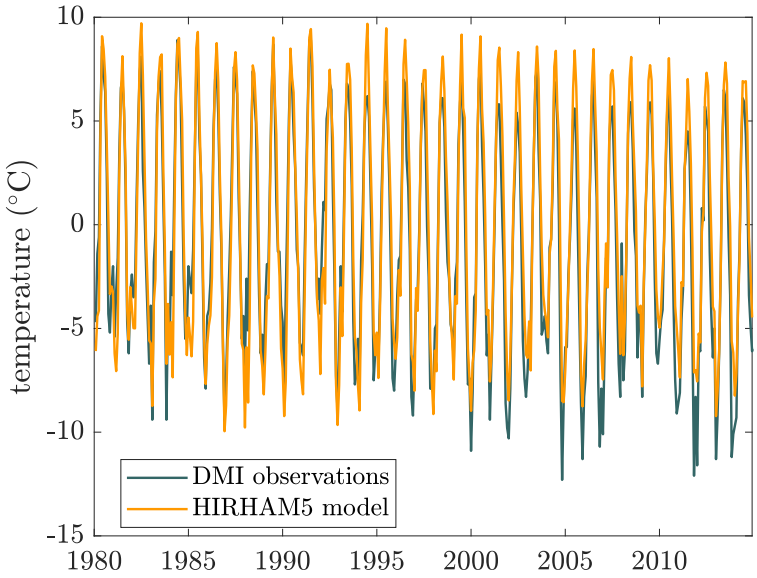


FIGURE 3.6: **HIRHAM5 vs DMI**
The modelled HIRHAM5 and the observed DMI temperature data series for the Tasiilaq station are shown for the time span 01/1980-12/2014.

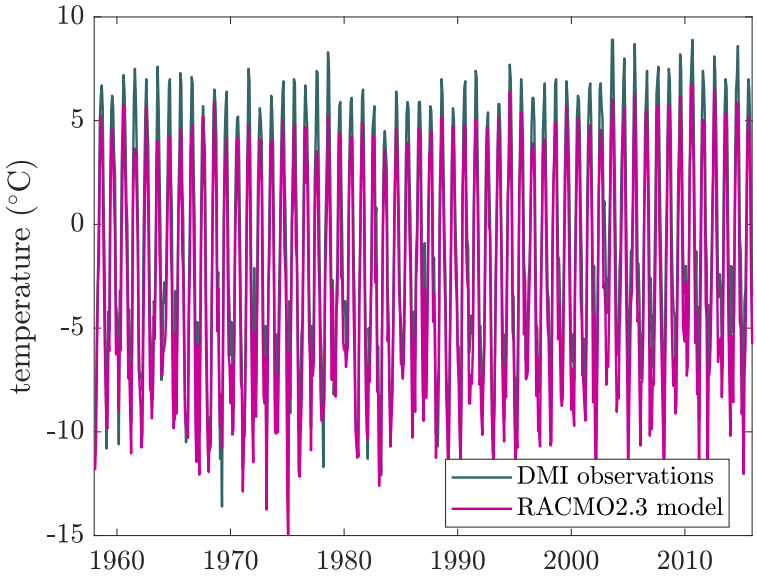


FIGURE 3.7: **RACMO2.3 vs DMI**
The modelled RACMO2.3 and the observed DMI temperature data series for the Tasiilaq station is shown for the time span 01/1958-12/2015.

## 3.5 $\delta^{18}$O as paleothermometer - the concept

The recovered ice cores from Renland 1988 and RECAP 2015 were analysed for water stable isotopes. As preparation, the ice is cut in samples of the desired sample size and further processed for the chosen measurement technique. Data of the 1988 core is available in 5 cm resolution from 1.6 m down to 124.3 m depth. Below, the ice was cut in 2.5 cm pieces and the last sample corresponds to a depth of 324.375 m. The samples were analysed using the $CO_2$ equilibration technique. The melted ice sample is brought together with $CO_2$-gas until the isotopic composition of the oxygen in the water and the gas are in equilibrium. Then the $^{18}$O-content in the gas is measured with a mass spectrometer.
The ice core from 2015 was continuously analysed between 3.3625 m and 584.0725 m depth. For the continuous flow analysis (CFA) technique long ice samples are gradually melted from one end. The meltwater is then analysed for $\delta^{18}$O using cavity ring-down spectroscopy, i.e. a laser absorption technique. Missing data in the 2015 record was linearly interpolated between the edging data points. In order to add values above the uppermost ice core sample, isotope measurements of the firn core A6, which was drilled 100 m north of the 2015 drill site, were included. Both isotope records were matched to the GICC05 timescale and are hereby and comparable.
The calibration of the isotope paleothermometer, i.e. the definition of the linear dependency between $\delta^{18}$O in the ice and mean annual surface temperatures is performed using the method described in Jouzel et al. (1997). Annual $\delta^{18}$O means were calculated from the isotope records for the past 1000 years. For the RECAP ice core, this includes measurements down to about 269 m. All data from depths <215 m were used from the Renland 1988 record. The annual $\delta^{18}$O-values were then converted into a temperature signal using the following linear relationship:

$$T = m \cdot \delta^{18}O + c \tag{3.20}$$

The parameters $m$ and $c$ are chosen by forcing the BTMs with the resulting 1000 year temperature records and fitting the result to the observed BTC. The fitting is done in a least square sense.

# Chapter 4

# Results

## 4.1 Densification

Hereafter the results of the Herron-Langway densification model are presented. Data from both cores were used to find one solution. The surface temperature was set to $T_s = -18.4°C$ which is the mean of both borehole temperature measurements of the firn layer down to 85 m. An accumulation rate of $\lambda = 0.42$ m water equivalent / year was derived from Johnsen et al. (1992). The model chooses the parameters $\rho 0$ and $\rho_{crit}$ and the two fudge parameters $f0$ and $f1$ according to a least square fit. The best fit model curve can be seen in Figure 4.1. The tuning parameter values found,

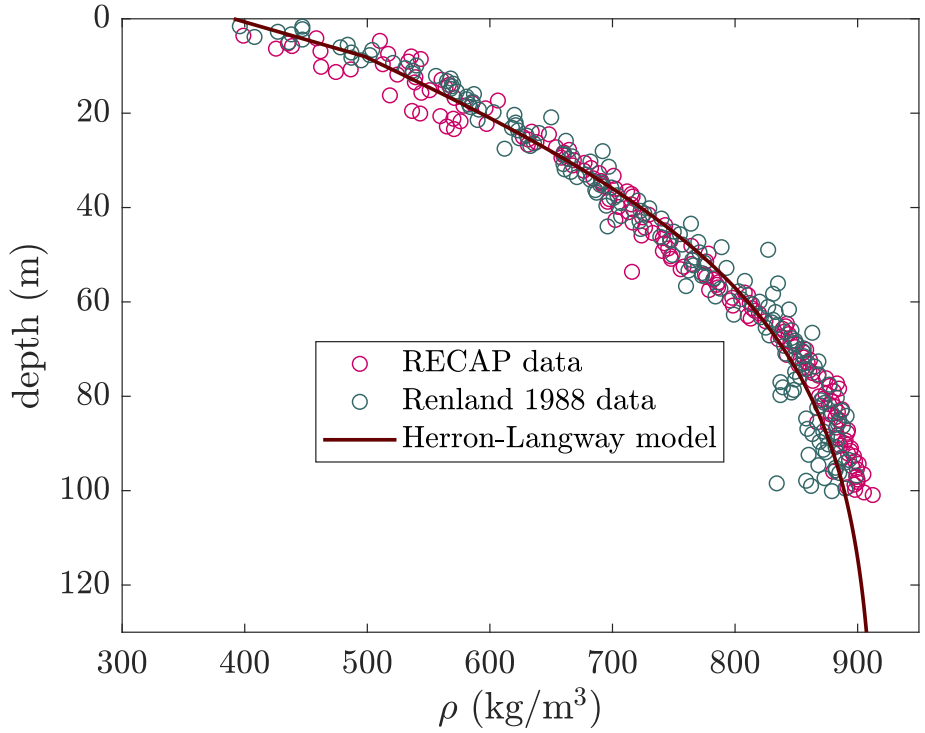


FIGURE 4.1: **Herron-Langway model fit to the density data points of both drill campaigns** .

are presented in Table 4.1. Those parameters correspond to a critical depth of $d_{crit} = 7.97$ m, a close-off depth of $d_{co} = 57.02$ m and a $\Delta$-age of 97 years. The air in the firn layer sums up to an air column of $V_{air} = 20.39\,\mathrm{m}^3$.

TABLE 4.1: Herron-Langway model tuning parameters

| **parameters** | **formula** | **best fit** | **unit** |
|---|---|---|---|
| initial density | $\rho 0$ | 391.084 | $kg/m^3$ |
| critical density | $\rho_{crit}$ | 497.782 | $kg/m^3$ |
| fudge factor for K0 | $f0$ | 0.7048 | - |
| fudge factor for K1 | $f1$ | 1.0744 | - |

### 4.1.1 3-stage densification

When plotting $ln(\frac{\rho}{(\rho_{ice}-\rho)})$ for RECAP a third stage of densification starting off from a density around 800 $kg/m^3$ (corresponds to $\ln[\rho/(\rho_{ice}-\rho)] = 1.92$) could be identified (Figure 4.2). It was tested if an adjusted Herron-Langway model with three

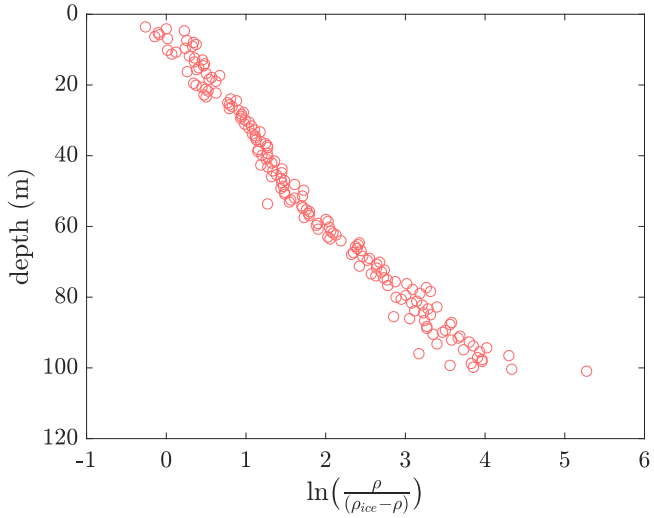


FIGURE 4.2: **Depth-($\ln[\rho/(\rho_{ice}-\rho)]$) data for the RECAP site** .

densification stages would yield a better fit. A third densification stage in the form of the second Herron-Langway stage was added. The model was allowed to choose the density at the transition from stage two to stage three freely and assigned a value of $\rho_{t_{2/3}} = 891.33\,kg/m^3$. However, the calculated sums of residuals (residual= $(\rho_{calc} - \rho_{obs})^2$) of both tested models differ by 0.4 only (see table 4.2). Therefore the 2-stage original Herron-Langway model with fewer degrees of freedom was used subsequently. A plot showing the graph of the 3-stage model and the corresponding parameters can be found in the appendix.

TABLE 4.2: Error estimates of density model variations

| **model** | **sum of residuals** | **unit** |
|---|---|---|
| 2 stages | $1.252590 \cdot 10^5$ | $(kg/m^3)^2$ |
| 3 stages | $1.252586 \cdot 10^5$ | $(kg/m^3)^2$ |

## 4.2 Flow profile

Several modifications of the original Dansgaard-Johnsen *kink-model* were tested comprising of the original *kink-model*, the *kink-model* with bottom sliding, a new *step-model* and a combination of each with a dead ice layer. The one that models the depth-age relationship best was found using a least-square method. Schemes, which depict the differences in the horizontal flow of the different models are given in the appendix.

### 4.2.1 RECAP

For the RECAP site, all age markers within the Holocene period were used for the fit and the sum of the residuals calculated to identify the best model. The observed annual layer thicknesses increase in greater depths (after Holocene), which indicates a thinning behaviour, different from the regular one. Calculated errors for each model variation are listed in Table 4.3. The corresponding model parameters and graphs are attached in the appendix. The *step-model* with a dead ice layer gives the best age

TABLE 4.3: Error estimations of flow models- RECAP

| **model** | **dead ice** | **sum of residuals** | **unit** | **model parameters** |
|---|---|---|---|---|
| kink | - | $3.892 \cdot 10^6$ | $years^2$ | 2 |
| kink +bottom sliding | - | $3.895 \cdot 10^6$ | $years^2$ | 3 |
| step | - | $7.496 \cdot 10^7$ | $years^2$ | 3 |
| kink | ✓ | $2.540 \cdot 10^6$ | $years^2$ | 3 |
| kink +bottom sliding | ✓ | $7.822 \cdot 10^5$ | $years^2$ | 4 |
| step | ✓ | $2.092 \cdot 10^5$ | $years^2$ | 4 |

fit. Figure 4.3 shows the model result together with the age fixpoints and the worse fitting *kink-model* outcome. The corresponding model parameters are given in Table 4.5 together with the parameters for the old drill site.

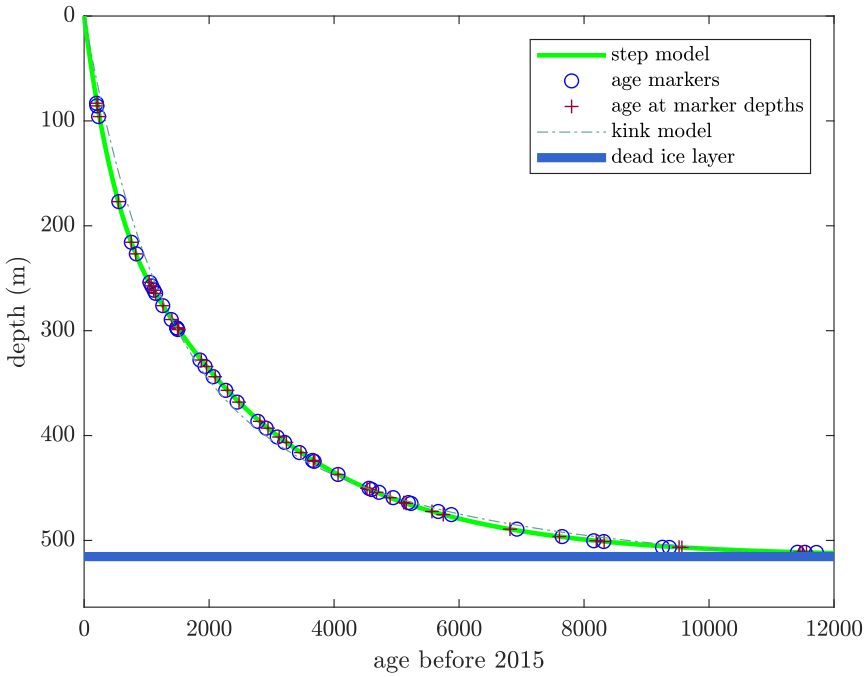


FIGURE 4.3: **RECAP ice flow fitted to the age markers**
The resulting age curve from the *step-model* is displayed on an ice equivalent depth scale. The beginning of the dead ice layer at 48 m above bedrock is indicated as well. The gray, dashed curve shows the Dansgaard-Johnsen *kink-model* curve. An accumulation rate of 0.33 m/year and a kink height of $h_{kink} = 217$ m were used for calculating this curve.

The calculated ages at the depths of the known markers are in good agreement with the observed ages down to a depth of 450 m. Below, the curve follows the shape of the markers, however, the estimated ages are younger than the age of the markers down to a depth of 500 m. Further below the model predicts older ages than the ones observed. The age estimate errors were compared to the GICC05 time scale uncertainties. Therefore the originally stated time scale uncertainties were corrected for the discovered 7-year offset of GICC05 at 1000 years b2k (before 2000) (Sigl et al., 2015). The step-model age predictions were within the uncertainty limits in ten out of the 45 used age markers. The matching calculations are evenly distributed over the whole Holocene age markers, i.e. the uncertainty can not be assigned to either the upper or lower part of the ice core. Using any of the other flow models resulted in less than three agreements between model error and timescale uncertainty.

### 4.2.2 Renland 1988

Age markers in the Renland 1988 were used down to a depth of 280 m, where Vinther et al. (2008) found an annual layer minima. Below, the layers get thicker indicating a flow different from the normal flow regime. Error estimates for all tested models are listed in Table 4.4. A diagram showing the different age curves and a table with the corresponding parameters are attached in the appendix.

TABLE 4.4: Error estimations of flow models- Renland 1988

| model | dead ice | sum of residuals | unit | model parameters |
|---|---|---|---|---|
| kink | - | $1.386{\cdot}10^7$ | $years^2$ | 2 |
| kink +bottom sliding | - | $1.388{\cdot}10^7$ | $years^2$ | 3 |
| step | - | $5.006{\cdot}10^7$ | $years^2$ | 3 |
| kink | ✓ | $8.500{\cdot}10^7$ | $years^2$ | 3 |
| kink +bottom sliding | ✓ | $7.518{\cdot}10^5$ | $years^2$ | 4 |
| step | ✓ | $2.879{\cdot}10^4$ | $years^2$ | 4 |

A *step-model* with a dead ice layer gives the best age estimation. The corresponding parameters are displayed in Table 4.5. As for the RECAP site, the *step-model* with a dead ice layer yields better results than the original *kink-model* as can be seen in Figure 4.4. The calculated ages at the depths of the known markers are in close

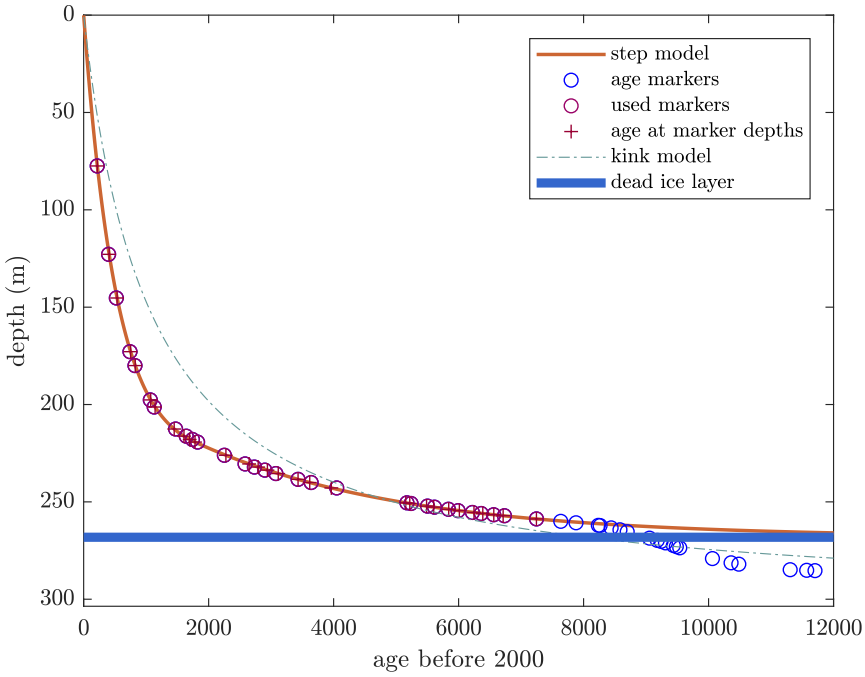


FIGURE 4.4: **Renland ice flow fitted to the age markers**
The resulting age curve from the *step-model* is displayed on an ice equivalent depth scale. The layer of ice, frozen to bedrock 35 m above bedrock is indicated as well. The gray dashed curve shows the best fit Dansgaard-Johnsen *kink-model* curve. The model finds an accumulation rate of 0.28 m/year and a kink height of $h_{kink} = 300$ m.

agreement with the observed ages. Comparing the model errors with the uncertainties of the GICC05 age estimate, 15 of the 30 modelled marker ages are within the limits of uncertainty. For the Renland 1988 site, model errors are mainly smaller than the uncertainty in the lower part of the ice core. Any other tested flow model produced age residuals, higher than the GICC05 counting uncertainty at the certain depth.

### Comparison of the two flow models

The parameters subsequently used for the two drill sites are given in Table 4.5. Remarkable is, that the predicted beginning of the dead ice layer at the Renland 1988 site is very close to the annual layer minima (depth$= 279$ m) found in the ice core. Further, the accumulation rates are within an acceptable range to the observed accumulation rates at Renland ($0.46 - 0.5$ m ice eq./year). The RECAP step depth of almost 280 m corresponds well with the peak height of one of the (bedrock) mountains enclosing the valley from which the core was drilled. The mountain is around 304 m high which translates to an ice depth of 290 m. The mountain on the other side of the valley is with 240 m not as high.

TABLE 4.5: Flow model parameters

| **parameters** | **formula** | **RECAP** | **Renland 1988** | **unit** |
|---|---|---|---|---|
| step depth | $H - h - d_{tot}$ | 279 | 240 | m |
| dead ice depth | $H - d_{tot}$ | 536 | 289 | m |
| dead ice layer thickness | $d_{tot}$ | 48 | 35 | m |
| step ratio | $fb$ | 0.29 | 0.16 | - |
| accumulation | $\lambda_H$ | 0.46 | 0.43 | m ice eq./year |

The step-model fit was recalculated using the relative error instead of the absolute error for the minimising criteria. The resulting model parameters are slightly different and can be found in the appendix.

## 4.3 Borehole temperature profile

In Figure 4.6 the measured temperatures of the two boreholes are displayed. The measurements of July 1988 started at a depth of 10 m. The 2015 measurements were performed twice. Once, before drill liquid was added down to a depth of 85 m, and again after the drilling was completed. As can be seen in Figure 4.6, the measurements in the wet RECAP borehole show some wiggles in the profile between 80 and 150 m. As those deviations from a smooth curve are likely caused by the dissipation of heat in the borehole from the drill liquid, all wet borehole measurements down to 150 m were not taken into account for analysis. The temperature sensor had a measurement uncertainty of 30 mK which is indicated with errorbars in this plot. In the following graphs the errorbars are not shown again, since the marker sizes are large enough to include the uncertainty.

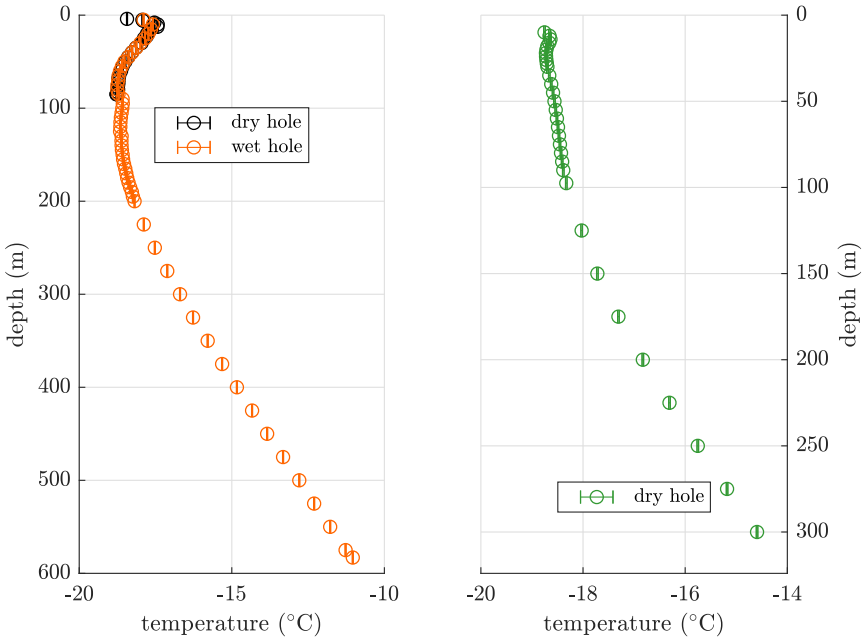


FIGURE 4.5: **Borehole temperature measurements**
The left graph shows the RECAP measurements. The dry borehole was analysed on 17/05/2015 and the fluid filled borehole on 15/06/2015. The right graph shows the Renland 1988 temperature data measured on 24 and 25/07/1988.

### 4.3.1 Isothermal forcing profile

The geothermal heat flux for the two locations was estimated within the spin-up phase of the model run. The models were forced with a constant surface temperature until the initial isothermal temperature curve had adjusted to a steady state solution. The constant surface temperature as well as the geothermal heat flux were tuned simultaneously in a least square sense in order to be in good agreement with the three lowest temperature measurement points. For RECAP, the one closest to bedrock was ignored and the three measurements above were used instead. Borehole temperature measurements were taken shortly after finishing the drilling. It is therefore likely that heat, produced while drilling the ice core had not been dissipated yet and influenced the measurements. Figure 4.6 shows the best fit steady state model results, which are subsequently used as initial conditions for the different surface temperature forcing scenarios.

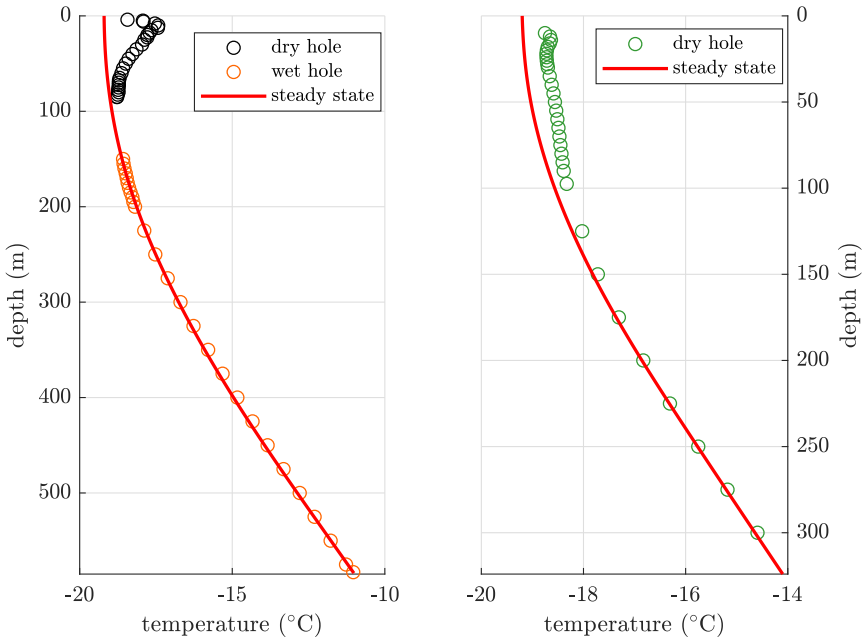


FIGURE 4.6: **Steady state borehole temperature curves**
The left graph shows the RECAP and the right the Renland temperature 1988 model curve.

The used constant surface temperature for both locations was -19.2°C. The heat flux value is found to be slightly different for the two drill sites. It is $Q_{geo} = 49$ mWatts ($misfit = 0.02$) for the RECAP site and $Q_{geo} = 51$ mWatts ($misfit = 0.02$) for the Renland 1988 site. The misfit was calculated using equation 3.19.

### 4.3.2 DMI station temperature forcing

Weather station data was available with a monthly resolution while the total timespan of each temperature series varies.

#### Tasiilaq

Starting with the steady state solution profile from Figure 4.6 the Tasiilaq forcing scenario was applied. Tasiilaq is a coastal station about 600 km south of the Renland peninsula. A temperature record of 120 years was available from this station. The whole temperature record was shifted to compensate for elevation and latitude differences before using it as upper boundary condition. $T_{shift} = -17.4°C$ was applied to the RECAP and $T_{shift} = -17.3°C$ to the Renland 1988 model. Calculated model errors are given in Table 4.6. Forcing the models with this data, the curves shown in Figure 4.7 were calculated. It seems impossible to model the small wiggles in the top

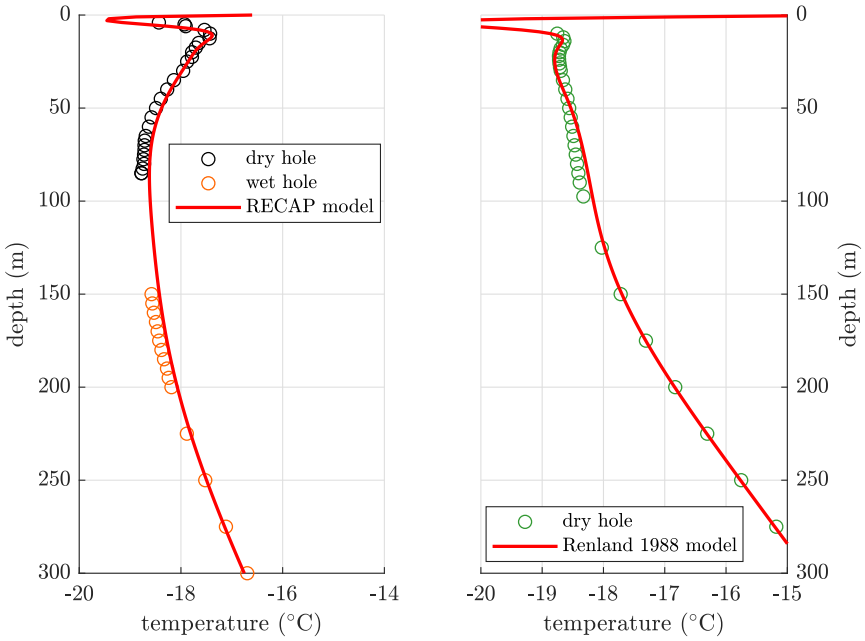


FIGURE 4.7: **BTM run with Tasiilaq forcing**
The left graph shows the RECAP and the right the Renland 1988 temperature model curve.

part while getting a good fit with the middle part for the RECAP model. Here the last summer warming is well modelled, but the temperatures are not cold enough between 30 and 200 m. In the Renland 1988 model the curve is too negative in the top part, after intersecting with the data points at 55 m the curve is slightly too positive down to a depth of 125 m where it meets the measurements again.

The Tasiilaq temperature record dates back to 1895 whereas the other two DMI stations only started recording in 1950. In those additional 55 years, the BTCs developed from the steady state solution to a curve, which can be seen in Figure 4.8. Since

this curve shows a great deviation from the steady state solution it was subsequently used as initial temperature curve for the following DMI model runs.

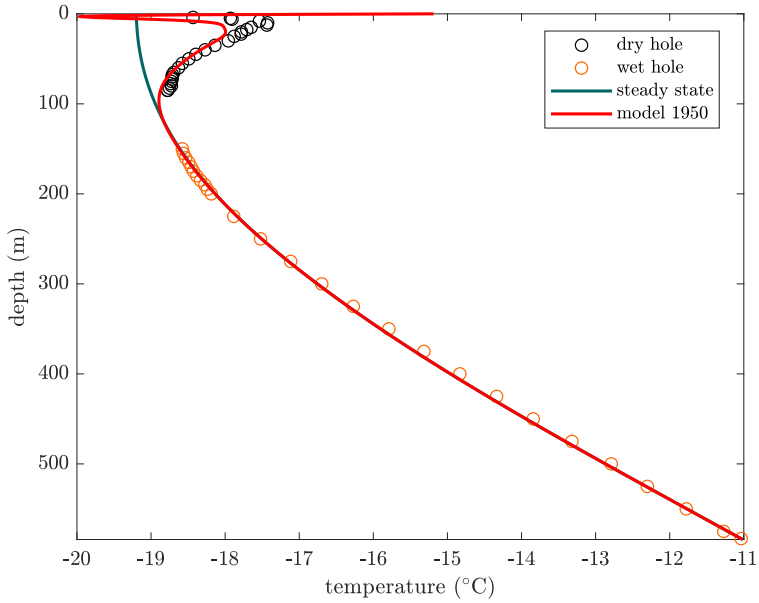


FIGURE 4.8: **BTM run with Tasiilaq forcing until 1950**
The shifted Tasiilaq temperature record from January 1895 until May 1950 is used as surface temperature forcing. A warming of the uppermost 150 m in response to the arctic warming in the early 20$^{th}$ century can be observed.

### Ittoqqortoormiit

Ittoqqortoormiit is the station closest to the Renland peninsula. It has recorded climate data since 1950. Hence, 38 years of monthly Ittoqqortoormiit forcing were applied to the Renland 1988 model and 65 years to the RECAP model. In order to adjust for the elevation difference between Renland and the station, the Ittoqqortoormiit temperature curve was shifted by $T_{shift} = -12.22°C$ in the RECAP model and by $T_{shift} = -11.38°C$ in the Renland 1988 model. The value for $T_{shift}$ was found using a least square fit. The results are given together with the other station outcomes in one table (Table 4.6) at the end of this section. The graphical outcome is plotted in Figure 4.9. It is obvious that the RECAP model is in closer agreement with the measurements than the Renland 1988 model. The BTC shape is too pronounced in the Renland 1988 model compared to the data points and only agrees with the measurements from a depth of 150 m downwards. Despite being too cold in depths between 70 and 150 m, the RECAP model curve follows the data points closely. The last summer warming in the top is estimated too warm in the model.

### Danmarkshavn

Danmarkshavn is the station furthest north, 600 km from the Renland peninsula. It has recorded since 1949, similar to Ittoqqortoormiit. The temperature shift applied

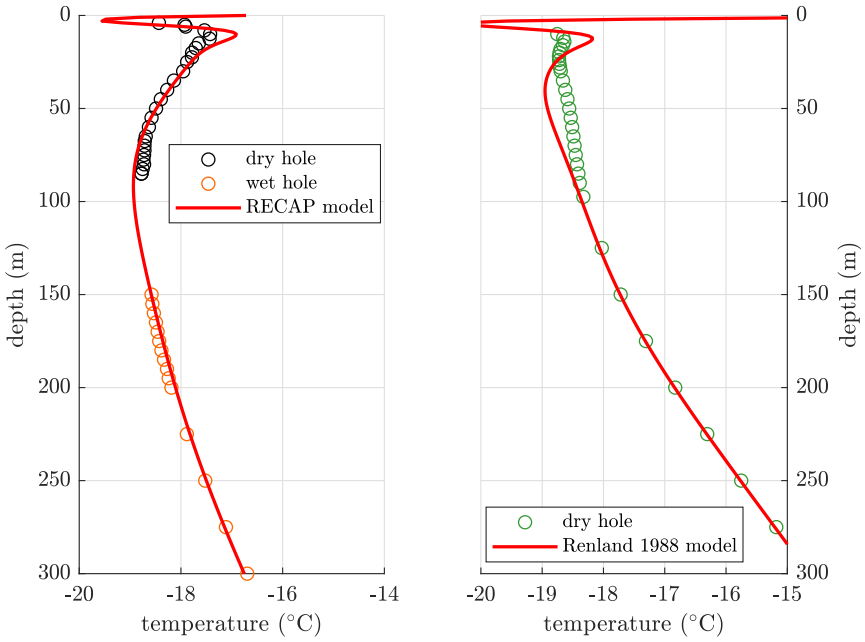


FIGURE 4.9: **BTM run with Ittoqqortoormiit forcing**
The left graph shows the RECAP and the right the Renland 1988 BTC.

to this data set was $T_{shift} = -6.35°C$ for RECAP and $T_{shift} = -6.37°C$ for Renland 1988 as can be seen in Table 4.6. The RECAP model outcome agrees well with the

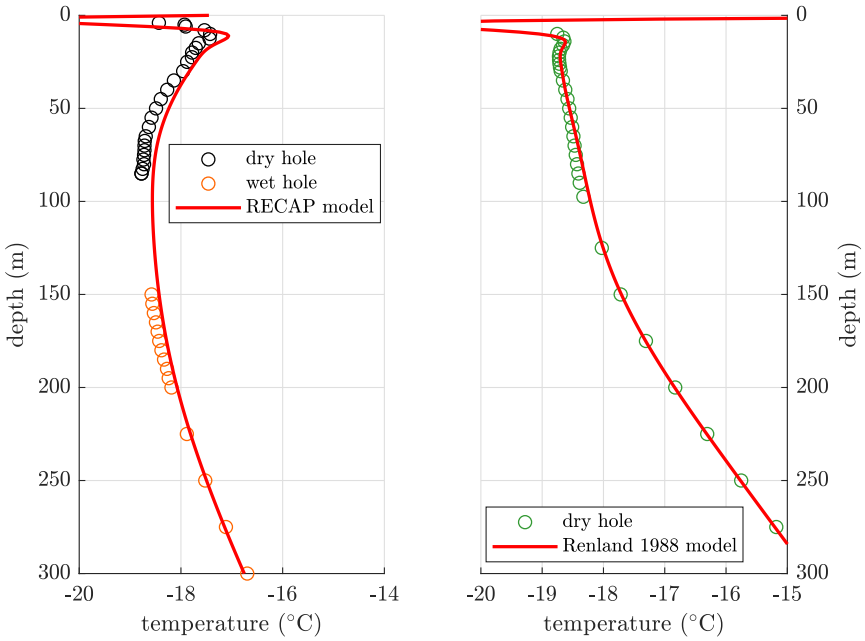


FIGURE 4.10: **BTM run with Danmarkshavn forcing**
The left graph shows the RECAP and the right the Renland 1988 temperature model curve.

data below a depth of 250 m. The top part is too warm in the model and the deviation with 0.5 °C large. The Renland 1988 model model is in very good agreement with the observations and only deviates slightly between 80 and 120 m.

**Comparison of DMI forcing scenarios and trend analysis**

All temperature shifts as well as the corresponding calculated misfits are given in Table 4.6. The total Tasiilaq forcing misfit ($misfit_{RECAP} + misfit_{Renland1988}$) is the

TABLE 4.6: DMI surface forcing adjustments and error estimations

| forcing | location | $T_{shift}$ °C | $misfit$ °C |
|---|---|---|---|
| **Tasiilaq** | RECAP | -17.40 | 0.02 |
| | Renland 1988 | -17.30 | 0.02 |
| **Ittoqqortoormiit** | RECAP | -12.22 | 0.03 |
| | Renland 1988 | -11.38 | 0.04 |
| **Danmarkshavn** | RECAP | -6.35 | 0.05 |
| | Renland 1988 | -6.37 | 0.01 |

smallest. Hence, monotonic trend analysis and corresponding linear slope estimates were performed on the Tasiilaq temperature data using a Mann-Kendall test and the non-parametric Sen's method (Gilbert, 1987). The results for the annual mean temperature in the three time periods 1895-2015, 1895-1987, 1988-2015 are shown in Table 4.7. No significant (significance level $\alpha = 0.1$) warming was recorded in the period 1895-1987. However, annual mean temperatures showed a significant ($\alpha = 0.001$) warming with a slope of $Q = 0.091\,°C$/year in the years between the drill campaigns. Monthly trend analysis results are given in the appendix.

TABLE 4.7: Tasiilaq annual temperature trend statistics

| trend parameter | unit | 1895-2015 | 1895-1987 | 1988-2015 |
|---|---|---|---|---|
| **Mann-Kendall parameter** | | 3.51 | 1.15 | 4.32 |
| **Probability of monotonic trend** | % | 99.9 | <90 | 99.9 |
| **Sen's slope** | °C/year | 0.010 | 0.004 | 0.091 |
| **lower limit 95% conf. interval** | °C/year | 0.005 | -0.004 | 0.058 |
| **upper limit 95% conf. interval** | °C/year | 0.015 | 0.013 | 0.120 |

**Universal Renland temperature history**

To give an approximate temperature history of the 20th century for the Renland peninsula the longest and well fitting Tasiilaq temperature record was tuned, to achieve an optimum, universal fit when used as input surface forcing in both models. The model runs with the Tasiilaq surface forcing produced a good fit but temperatures, which are too warm in the middle part of the borehole. The observed arctic warming event from 1920-1960 seems too pronounced in the Tasiilaq forcing scenario (Johannessen et al., 2004). To check, if the fit can be improved when accounting

for that, an additional tuning parameter was introduced to the model set-up. A cooling parameter ($T_{cooling}$) was added for the time span 1925-1964. Overall temperature shift $T_{shift}$ and $T_{cooling}$ were tuned simultaneously and the models calculated average parameters of $T_{shift} = -17.2\,°C$ and $T_{cooling} = -1.0\,°C$. The calculated curve misfits sum up to a total misfit of $0.04°C$. The RECAP borehole temperature predictions improve visibly whereas the Renland 1988 model curve shows a slight negative offset in depths between 30 and 80 m.
However, using the mean of the optimum values from the Renland 1988 and RECAP model yielded similar results. An overall temperature shift of $T_{shift} = -17.35\,°C$ and no additional cooling factor resulted in a total misfit of $0.04°C$ as well. The RECAP model fit decreased but the Renland 1988 fit improved. Since the introduction of an additional parameter did not provide substantial reduction of the misfit, the simple shifting of the entire Tasiilaq time series is presented in the following figure. Figure 4.11 shows annual means of this one-tuning parameter universal temperature series and the BTCs that developed when the models were forced with it.

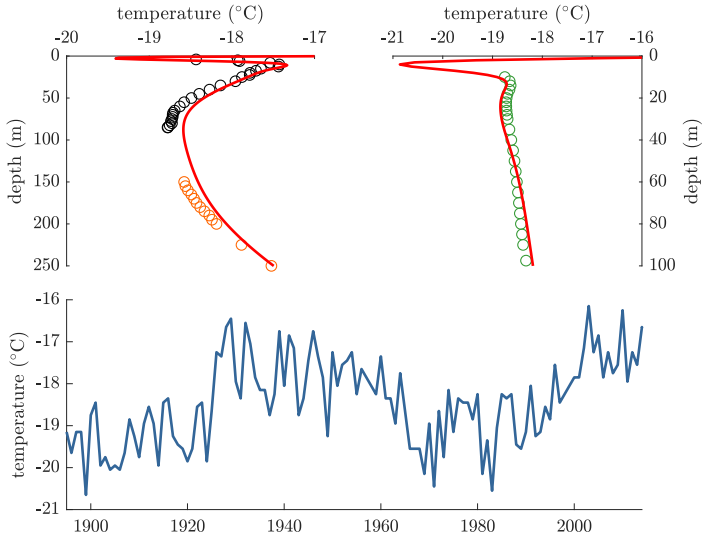


FIGURE 4.11: **Estimate of Renland temperature history**
The top left plot shows the RECAP BTM result and the top right plot the Renland 1988 model result. Both models were forced with monthly data of the annual mean temperature history seen in the lower half of the figure (Renland 1988 model only forced until 06/1988.)

### 4.3.3 RCM temperature forcing

Instead of using observational data, the models were then forced with the output of a Regional Climate Model. In comparing the BTM outcome with the observed BTCs it is possible to assess the RCM performance over Renland. The Tasiilaq surface temperature forcing was applied from 1895 until the year, for which RCM data was available.

#### HIRHAM5

The HIRHAM5 Regional Climate Model is only used for the RECAP model since the HIRHAM5 model period spans from 1980 to 2014 only. The first five months of year 2014 were repeated to have an input until the date of the RECAP drilling. First, the model outcome was used directly as forcing and afterwards a temperature shift was applied as was done with the DMI station data. The temperature shift that gives the best model result is $T_{shift} = 2.08°C$. The misfit for the directly applied version and the adjusted temperature series can be found in Table 4.8. As can be

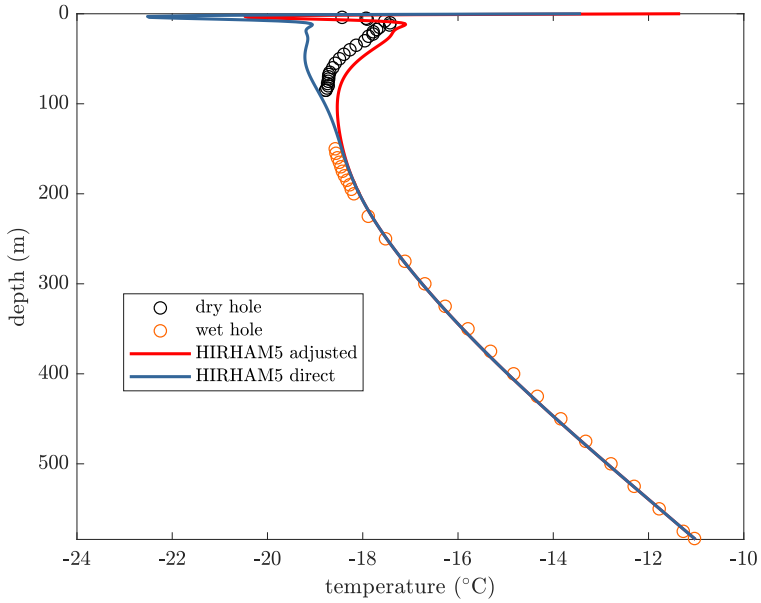


FIGURE 4.12: **RECAP BTM run with HIRHAM forcing**
The adjusted model was corrected with a positive temperature shift of 2.08°C.

seen in Figure 4.12 when applying the RCM outcome directly, the model calculated a BTC which is too cold for the RECAP site. The maximum deviation of 1.5 °C of the model from the data happens during the last summer warming. After adjusting, the temperatures above 80 m are too warm by half a degree Celcius but the overall deviation is reduced.

### RACMO2.3

The RACMO2.3 model timespan is from 1958 to 2016. Therefore it was possible to use it as surface forcing input for both models. As before, the RACMO2.3 model outcome was used directly as forcing and was adjusted later on. The misfits for the direct use and the misfits after adjustment are given in Table 4.8. Directly applied,

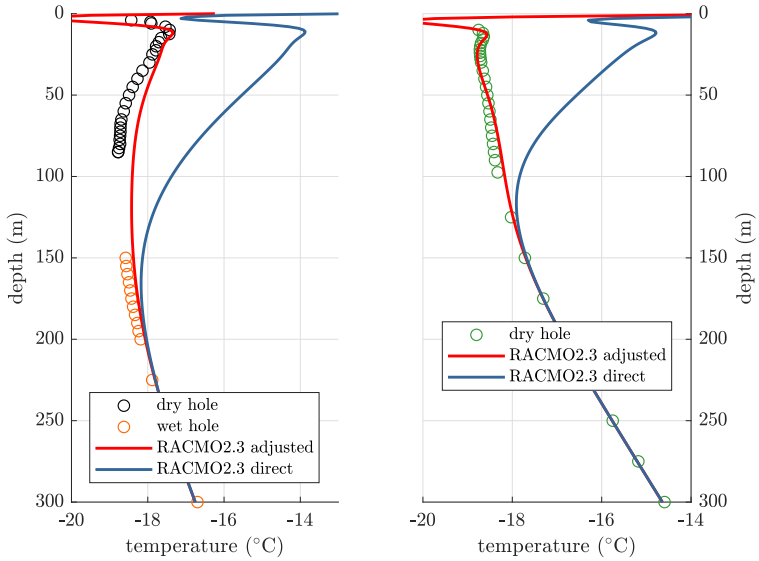


FIGURE 4.13: **BTM run with RACMO2.3 forcing**
The left graph shows the RECAP (adjusted with $T_{shift} = -3.58°C$) and the right the Renland 1988 (adjusted with $T_{shift} = -4.10°C$) temperature model curve.

the RACMO2.3 model outcome led to a warmer borehole temperature curve than the one observed. The maximum deviation around the last summer warming is 3.5 °C for both sites. Furthermore, the outcome of the Renland 1988 site is too curvy compared to the data. After applying the temperature shift the modelled curve resembles the observations better. However, the top part is not as linear as in the measured data. The shape of the RECAP model is of the same kind as the measured curve. Yet shows a positive offset, even after correction. When adjusted, the model outcome meets the last summer warming but does not match the observations further down.

TABLE 4.8: RCM direct and adjusted error estimations

| **forcing** | **location** | $T_{shift}$ °C | $misfit$ °C |
|---|---|---|---|
| **HIRHAM5** | RECAP | - | 0.15 |
| | RECAP | 2.08 | 0.06 |
| **RACMO2** | RECAP | - | 0.27 |
| | RECAP | -3.58 | 0.06 |
| **RACMO2** | Renland 1988 | - | 0.39 |
| | Renland 1988 | -4.10 | 0.01 |

### Reanalysis data ERA-20C

ERA-20C reanalysis data was tested in the borehole model but performed worse than RCM or observational data. The data series comprise of monthly mean two meter above surface temperature for the period 1900-2010. When compared against the Tasiilaq temperature record of the same time span both data series showed a good correlation ($R^2$=0.91). However, the temperature offset between the data sets is -2.9 °C with the ERA-20C mean being colder. This is a larger discrepancy than what was calculated for the two RCM models. A reason might be the coarse horizontal resolution of 125 km of the global ERA-20C data set. This requires a gradual elevation increase near the coast which then results in lower elevation than actual elevation. In other words, locations of the RECAP or Renland coordinates on the ERA- Greenland, do not resemble the real site characteristics in terms of sea proximity, elevation and ice cover. Therefore the borehole temperature model results are not presented in this thesis.

## 4.4 Linear dependency between $\delta^{18}$O and temperature

Once the BTMs were set up they could be used to find the best parameter estimates for the linear dependency between temperature and isotopic composition of the ice (equation 3.20). Different values were tested and the ones that yielded the smallest misfit were then used to translate the isotope records into a temperature history.

### 4.4.1 Calibration of the paleothermometer

The RECAP isotope measurements of the core were available up to a depth corresponding to year 2013. Isotopes from a depth above the 2013-depth were sampled in firn cores. Here, averages of the isotope samples from the firn core A6 corresponding to the year 2014 and 2015 were added to the yearly average values of the ice core. The core A6 was drilled in close proximity to the RECAP drill site. A 1000 year data series of annual mean isotope values was used for the model run. The fit was again performed in a least square sense and the misfit calculated as in equation 3.19. Since annual average values of isotopes were used, the temperature data from the uppermost 20 m are excluded from the least square calculations. Seasonal signals can be found down to a depth of 20 m which can not be resolved with annual isotopic means (Cuffey and Paterson, 2010).

The RECAP BTC depicts too warm temperatures below a depth of 50 m. Above, the modelled temperatures are too cold compared to the data and the maximum deviation is around half a degree. The curve fits well in the deeper part of the borehole. The Renland 1988 BTC instead shows a slight offset towards a warmer deeper part. It also has a more pronounced curving than the data. Outstanding is a cold spot in a depth of roughly 25 m. The curve between 50 and 150 m is well in agreement with the observed temperatures.

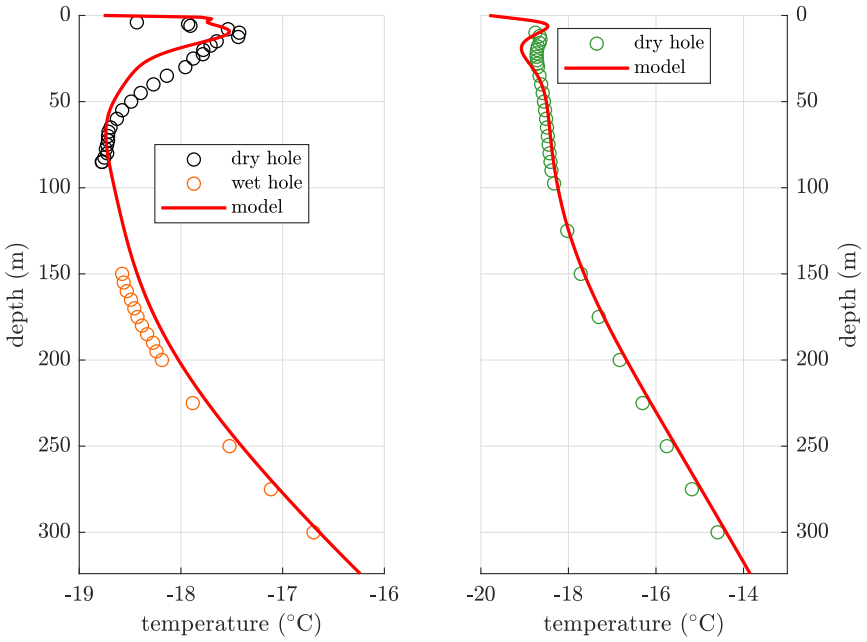


FIGURE 4.14: **BTM run with isotope forcing**
The left graph shows the RECAP and the right the Renland 1988 model results.

The best fit solution develops the two equations for the temporal relationship between mean annual surface temperature ($T_s$) and mean annual $\delta^{18}$O:

$$T_s = \begin{cases} 1.44 \cdot \delta^{18}O + 19.9 & \text{for RECAP} \quad (4.1) \\ 1.36 \cdot \delta^{18}O + 18.6 & \text{for Renland 1988} \quad (4.2) \end{cases}$$

The corresponding best fit misfit for RECAP is $misfit = 0.03\,°C$ and for Renland 1988 it is $misfit = 0.03\,°C$. Those misfits are of the same order of magnitude than the misfits calculated for the DMI or RCM model runs.

### 4.4.2 $\delta^{18}$O translated into Holocene temperatures

Equations 4.1 and 4.2 were used to translate the isotope records of the two ice cores into a temperature history. In Figure 4.15 the results are shown for the Holocene period. Annual means as well as ten-year averages are plotted. Since the accumulation rate was assumed to be constant, and the ice cores are rather short, the found temperature-$\delta^{18}$O relationship is only applicable for the Holocene, when overall climatic conditions were relatively stable. The uppermost plot shows temperatures calculated from the RECAP ice core isotopes and the central plot the Renland 1988 equivalent. The annual average curve shows larger variability for the RECAP temperature history. The variability of the RECAP curve steadily decreases while going back in time. In the Renland 1988 plot the variability decreases as well until the annual average curve almost matches the 10 year average curve for the period 4000-8000 years b2k, but increases again in earlier years. Comparing the 50 year smoothed

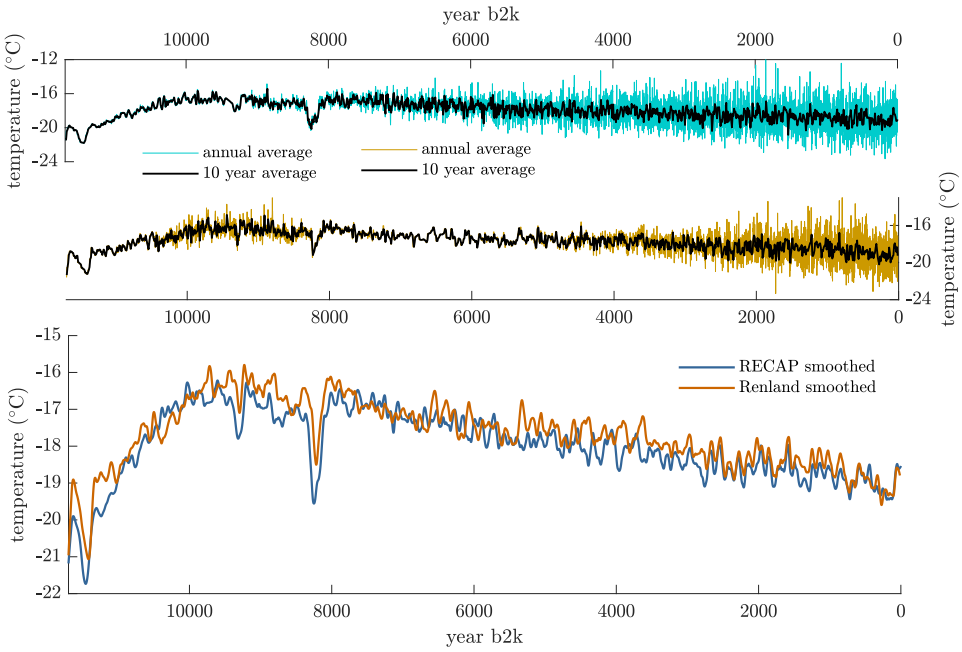


FIGURE 4.15: **Isotope records translated into temperatures**
The two upper graphs show the Holocene temperature histories derived from the RECAP and Renland 1988 $\delta^{18}$O isotope records, respectively. The lowest plot shows the two curves in a 50-years smoothed version together in one plot.

curves in the bottom plot, the Renland 1988 curve indicates slightly warmer temperatures throughout the entire Holocene compared to the RECAP curve. The offset between the two curves range from a maximum of -2.5 to 1 °C. The small scale dynamics of the curves are different. However, their overall behaviour is similar. Both graphs start out around -19 °C and increase until 9,500 y b2k to temperatures around -16 °C before they decrease with a higher rate than before to values below -21 °C. At 8,200 y b2k, 9,300 y b2k and 11,400 y b2k both graphs show sharp drops of more than one degree Celsius. Between around 3,200 y b2k and 7,800 y b2k the two curves are slightly shifted horizontally, i.e. the peaks and lows of the two curves do not lie on top of each other. Before and after this period, the matching of the two graphs is good.

Figure 4.16 shows a close-up of the two isotope-derived temperatures of the 20$^{th}$-century. Additionally, the Renland temperature history of section 4.3.2 is plotted for the same time period from 1900-2015. Shown are the 12-year Gaussian-smoothed curves of the annual mean temperatures. Overall, the curves follow the same pattern and stay within a temperature range of -20.5 to -17 °C. The two isotope-temperature curves are in closer agreement than the tuned weather station data. The 1930s warming event is clearly visible in all curves when comparing any of the three to the mean of the Renland temperature estimate. Moreover, an obvious temperature increase starting from 1980 can be observed.

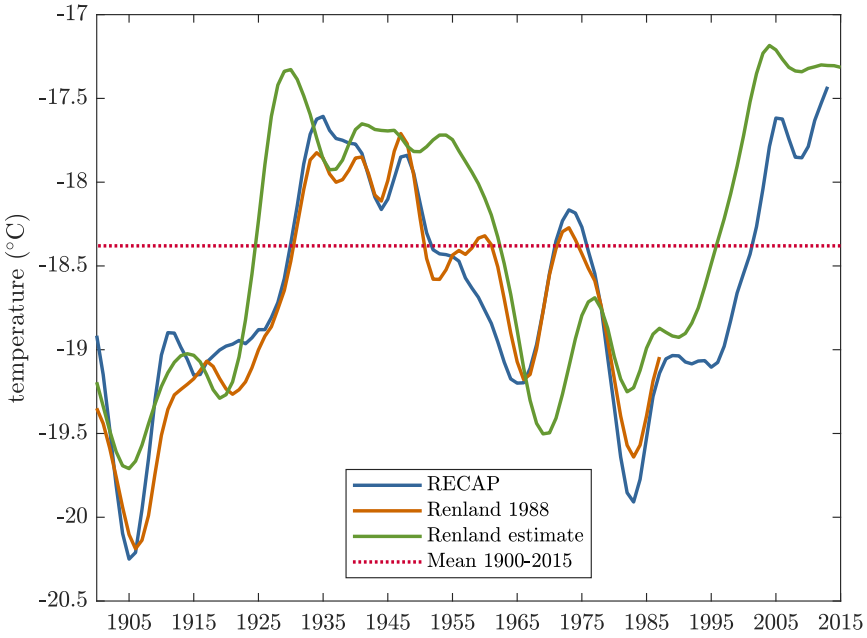


FIGURE 4.16: **Renland temperature estimates for the period 1900-2015**

The graph shows the two temperature records derived from the isotope records of the two ice cores as well as the Renland temperature estimate obtained from the Tasiilaq weather station record. Displayed are 12 year Gaussian-smoothed versions of the annual mean time series. Additionally, the mean temperature of the universal Renland temperature history of those 115 years with -18.38 °C is indicated.

# Chapter 5

# Discussion

## 5.1 Best fit analysis

### 5.1.1 Density model

When evaluating ice core density data, it must be considered that measurement errors will skew the data towards lower densities.
The Herron-Langway model is a semi-empirical model, widely applied due to its simplicity and the low amount of necessary input parameters. The best fit model in this thesis is in good agreement with the data down to a depth of 80 m. In greater depths, the model calculates lower densities compared to measured densities. To exclude the possibility that a third densification stage with different parameterisations minimises this deviation, a third stage in the same form as the Herron-Langway second stage was introduced. This approach was discarded since the model misfit improved only insignificantly. Input parameters, incoherent with observations were tested to see if the model could be forced to fit. However, improving the fit in the lower part would yield greater offsets in the top. It seems as if the applicability of the Herron-Langway model for the Renland site is limited. The Greenlandic density measurements which were used together with Antarctic data in developing the model, were all taken at inland sites where summer melting is rare. The Renland cores however show a great number of meltlayers. Melting, percolation and refreezing influence the densification process and should therefore be accounted for in the used model. An example would be the densification model of Reeh et al. (2005) that takes ice lenses stemming from melting into account. However, the application is beyond the scope of this thesis.

### 5.1.2 Flow model

The original Dansgaard-Johnsen *kink-model*, or modifications accounting for basal melt and sliding, were successfully applied for modelling the flow regimes at the Greenlandic deep drill sites Camp Century, DYE-3, GRIP, NGRIP and NEEM (Dansgaard and Johnsen, 1969; Dahl-Jensen, 1998; Johnsen et al., 1995; Dahl-Jensen et al., 2003; Buchardt, 2009). However, this model approach does not yield a good fit for

the Renland Ice Cap. Instead, a *step-model* approach, including a dead ice layer calculates good age estimates for both drill sites. However, modelled age misfits exceed the uncertainty estimates of the GICC05 timescale in half or more of the used age markers. Other flow models instead, only matched the uncertainty range at three or less observation depths. Hence we can assume that the prevailing flow regime at the ice cap is best resembled by a step-model. Counting annual layers is readily feasible within the Holocene period which explains the small uncertainty values. The maximum uncertainty of used age markers at the Renland 1988 site is 35 years and 106 at the RECAP site. Modelling ages within the uncertainty range at all observation depths is therefore an ambitious goal, that might not be achievable with such a few-parameter model.

When looking at the radar echogram between the two field sites (Figure 1.2) a dark layer near the bedrock followed by a lighter layer adjoining the bedrock can be identified. Identification of layers in a radio echogram can be attributed to differences in density, conductivity and fabric which influences the ice's reflectivity. Because the near bedrock layers can clearly be distinguished from the ice flowing above, it is possible that this ice has different flow characteristics. In fact, summing up those two layers at the RECAP drill site result in a thickness of roughly 50 m which is very close to the model predicted dead ice layer of 48 m. This supports the implementation of the dead ice layer in the model for the RECAP site.

The radio echogram for the Renland site does not show such outstanding near-bedrock layer anomaly. When plotting the counted annual layers of the two cores, an increase in annual layer thicknesses from a depth of 279 m and 553 m downward can be observed for Renland 1988 and RECAP, respectively (Figure 5.1). This indicates a flow contradicting a regular flow scheme. When plotting the annual layer thicknesses resulting from the best fit *step-model*s, the curves are in good agreement for the RECAP site. The curves for the Renland site match well down to a depth of 220 m. The modelled curve then shows an indent which is not observable in the measured layer thicknesses. This is due to the step assumption in the model set up. Despite this kink, the curve follows the overall sharply decreasing trend in the observed layer thicknesses. The flow model suggests a dead ice layer thickness of approximately 35 m. This deviates from the observed layer minima by ten meters. Fitting the flow model with less age markers (down to a depth of 264 m) yields a dead ice layer of 49 m instead. This would match the beginning of the layer thickening. However, using age markers down to 280 m yields a slightly better fit. A plot showing both layer thinning curves can be found in the appendix. It shows, that both models are very similar down to a depth of 225 m, where the observed annual layers decrease rapidly. The ice at 225 m is about 2250 years old.

In assuming a dead ice layer in general, the parameters used for the borehole temperature modelling are influenced substantially. Since the flow then does not reach down to bedrock, the ice frozen to the bed acts as an insulator, preventing cold temperatures from above from cooling the ice sheet at great depths. Thus, the assumed

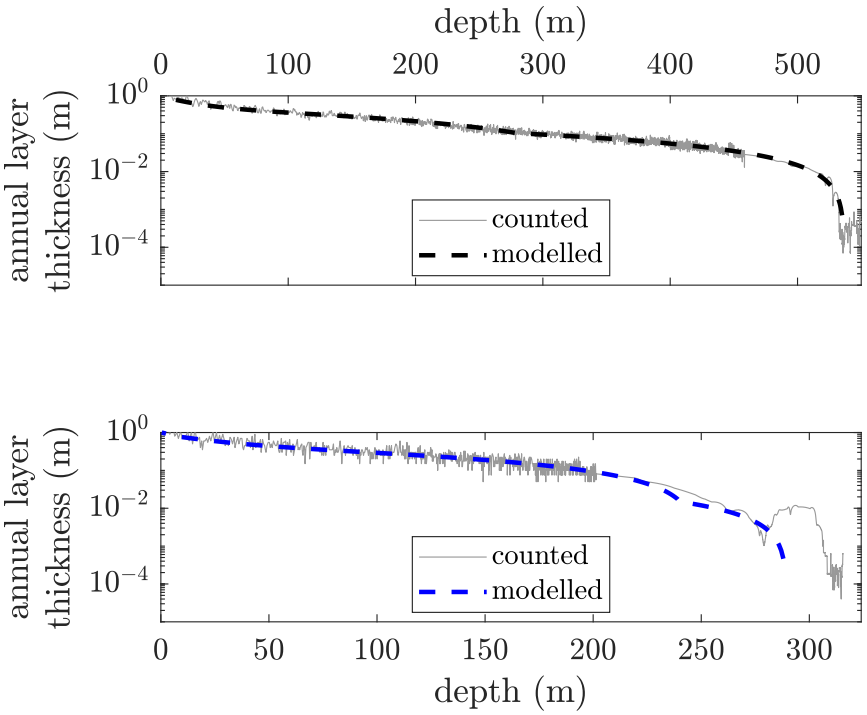


FIGURE 5.1: **Counted and modelled annual layer thicknesses**
The upper plot shows the RECAP site. The lower plot shows the annual layers at the Renland site and the corresponding modelled layer thicknesses. Note the layer minima at depths of 536 m and 279 m.

geothermal heatflux will be lower, when adding a dead ice layer to the flow model.

One might argue that the *step-model*, with a jump from one constant flow regime to another constant flow is physically unreasonable. However the strength of this model lies within its simplicity itself. The ice flow at the Renland Ice Cap is undoubtedly not comparable to the flow of the main ice sheet. Otherwise, the hitherto successfully applied *kink-model* would yield a good fit with the observed ages. Hence, the flow is somewhat more complicated. Nevertheless it is possible to get a reasonably good fit with a model, which only uses four degrees of freedom. Hereby, the simple *step-model* fulfills its function in matching the identified age data points. It is therefore a good conceptual model despite its crude simplifications of a rather complicated flow regime. Other works have used a nested flow model consisting of a large scale model providing boundary conditions for a fine scale model (Huybrechts et al., 2007; NEEM, 2013). Those models take upstream ice, stemming from another location into account and require an understanding of the overall flow regime of the ice sheet of interest. Currently such an ice cap flow model is under development but not ready to be used in this work.

### 5.1.3 Borehole temperature model

The model runs with input data from the DMI weather stations are compared in this section to evaluate the eligibility of the utilized borehole temperature model.
In general, a negative temperature shift of the model input data obtained from the

weather stations is anticipated. Latitudinal and elevation corrections are necessary when comparing temperature data from different locations. Since all DMI stations are within 70 m above sea level and the drill site locations are at an elevation of over 2 km, a temperature shift of several degrees is within expectation. This topographic elevation change is different from an elevation difference within the atmosphere, which distinguishes this rate of temperature change from rates observed within the atmosphere. Hanna et al. (2005) describe this phenomenon with *surface lapse rates* over ice sheets instead of the free atmospheric lapse rates. Furthermore, latitudinal corrections have to be taken into account. Those latitudinal temperature gradients strongly depend on the incoming solar radiation and are therefore different in the various climate zones of the earth and even on smaller spatial resolution. Steffen and Box (2001) calculated a mean annual latitudinal temperature gradient of $-0.78\,°C/1°\text{N}$ for the western slope of the Greenlandic ice sheet and a gradient of $-0.82\,°C/1°\text{N}$ for Eastern Greenland. The values are qualitatively supported by the findings of this thesis. It has been demonstrated that the higher the latitude of the input data station, the smaller the negative temperature shift that is necessary to obtain the best fit for the modelled temperature curve. A backward calculation of the surface lapse rates is performed to compare them to existing literature values. Taking the latitudinal corrected best-fit temperature shifts of the three DMI model runs one can calculate elevation temperature gradients. Those are called surface lapse rates and are given in Table 5.1.

TABLE 5.1: Surface lapse rates calculated from best-fit $T_{shift}$.

| **forcing** | **location** | $T_{shift}$ * °C | **surface lapse rate** °C/km |
|---|---|---|---|
| **Ittoqqortoormiit** | RECAP | -11.55 | -5.11 |
| | Renland 1988 | -10.71 | -4.72 |
| **Tasiilaq** | RECAP | -12.74 | -5.59 |
| | Renland 1988 | -12.63 | -5.53 |
| **Danmarkshavn** | RECAP | -10.83 | -4.67 |
| | Renland 1988 | -10.85 | -4.66 |

* latitude corrected to the borehole locations with the Eastern Greenland latitudinal gradient from Steffen and Box (2001)

Erokhina et al. (2017) presents mean annual slope lapse rates in a range from 5.9-8.2 °C/km for the Holocene period. Besides the annual slope lapse rates Hanna et al. (2005) and Erokhina et al. (2017) find lower summer slope lapse rates of 4.2-6.2 °C/km. The values obtained in this thesis are smaller than the annual values by at least 0.3 and maximum 1.2 °C/km but lie within the range of the summer month values. The deviation might be due to different observation periods that are used for the calculations. Further, it can be argued that cooling with height does not happen as fast in the peninsula region as if it were a location on the main ice sheet with

comparable elevation. The fjord might influence and dampen the cooling rate. The earlier presented literature lapse rate values were calculated at the coast. Sea ice, stemming from the Arctic and transported southward by the Fram Strait, might induce comparably cold summers at the Eastern coast whereas the fjord area does not experience summer sea ice. This might explain the lower temperature difference indicated by the lower surface lapse rates.

Overall it seems the origin of the misfit of the model lies within the surface temperature data. Tuning the Tasiilaq temperature record enables an optimum fit with both observed borehole temperatures. It can therefore be concluded that the herein presented set up can be used to model the borehole temperature provided, that good estimates of the surface temperature history are available. Further improvement might be accomplished by including an improved density model and changing accumulation rates which was done in models for other deeper boreholes (Vinther et al., 2009a). It must be kept in mind that the final uncertainty of the model temperature estimates comprise of uncertainties of dating, measurement accuracy of density and climate data and the uncertainties of the model parameter estimates. Further it should be noted, that the measured temperature profile might be influenced by the drilling method and the drill liquid and can thus contain uncertainties as well.

## 5.2 Comparison of Renland 1988 to RECAP 2015

The borehole temperatures were modelled for the sites Renland 1988 and RECAP 2015 using a universal density model and identical temperature diffusion assumptions. The implemented flow models are alike, but use different values for the model parameters. Nonetheless, the resulting BTCs are very distinct. The origin of this curve deviation can therefore be assigned to the surface forcing, more precisely to the time period of the temperature input. The warming in the uppermost 80 m of the RECAP borehole is not observed in the Renland 1988 borehole. It was therefore induced within the 27 years between the two drill campaigns. Hence, the Renland peninsula experienced a sustained warming during this time. These observations are supported by the results of the trend analysis test of the Tasiilaq temperature time series. A significant trend of 0.95°C/year is calculated for the period 1987-2015. The earlier time period does not show a significant positive trend.

When comparing the calculated lapse rates between the RECAP 2015 and the Renland 1988 model of section 5.1.3 one finds smaller lapse rates for the Renland 1988 model. This can be an indicator for more pronounced warming along the coast compared to the ice cap region. The temperature difference between the coastal DMI stations and the drill site is larger in 2015 which demands for higher lapse rates.

Since the significance and slope calculations of Table 4.7 are calculated from the Tasiilaq temperature dynamics, they show the temperature behaviour of the coast and should merely be taken as an indication for Renland temperature behaviour.

In order to exclude the possibility that the model curve deviation stems from another source than the surface forcing, the evolution of the RECAP temperature curve is shown in Figure 5.2. The RECAP model was forced with Tasiilaq input data and the curve shape is plotted in nine year steps from 1988-2015. Additionally, the Renland 1988 model was forced with Tasiilaq input data until 2015 and the hypothetical evolution of the curve can be observed in Figure 5.2. The red curve in the Renland 1988 plot follows the same shape as the borehole temperatures measured in 2015. If a borehole was drilled in 2015 at the Renland 1988 site, the measured BTC would look like this.

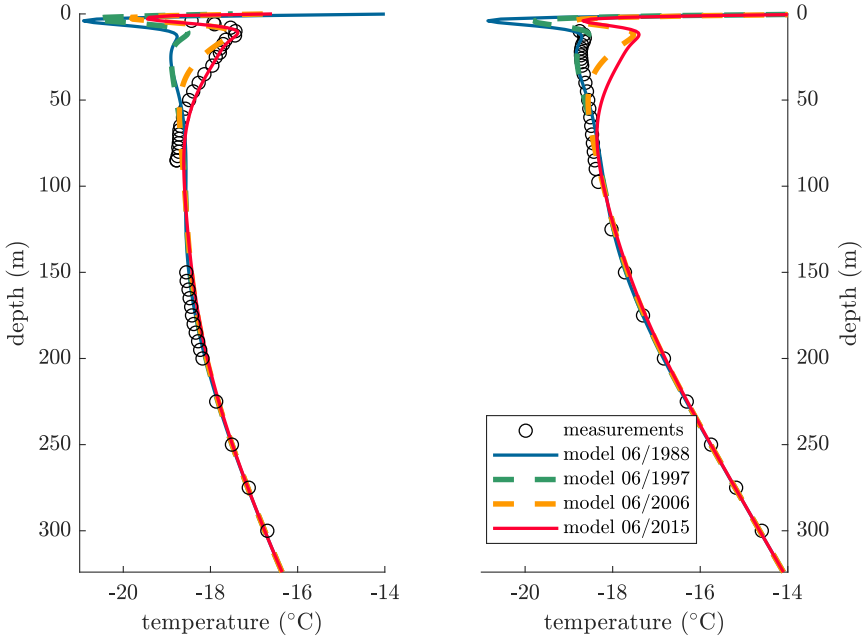


FIGURE 5.2: **The evolution of the BTC in both boreholes**
The left plot shows the evolution of the RECAP BTC from 1988 to 2015 in nine year steps. The right plot shows the hypothetical evolution of the Renland 1988 BTC with the same temporal resolution. The Tasiilaq temperature record was used to force the model from above and was corrected with the same temperature shift as in the previous model runs.

When estimating the 20$^{th}$-century temperature record for the Renland peninsula (Figure 4.11) two temperature records produce BTCs with the same total minimum misfit of 0.04 °. One temperature history estimate was obtained in shifting the Tasiilaq temperature record by the mean of the observed optimal $T_{shift}$ for Renland 1988 and RECAP. The other one included a cooling factor to account for the 1930s warming which was simultaneously tuned with the overall shift. Both tuning methods produce the same misfit, but the two scenarios favour either one or the other model outcome. When applying the mean temperature shift $T_{shift} = -17.35\,°C$ the fit

of the Renland 1988 model improves and when adding the cooling factor, the RECAP model result improves. It is therefore not possible, to make exact predictions about the 20$^{th}$-century temperature history of the Renland peninsula. The proposed Renland temperature record inherits the temperature behaviour and variability of Tasiilaq that is situated 600 km further south. The suggested Renland temperature record should therefore merely be interpreted as an indicator for the actual temperature record. From the results discussed in this thesis it can be concluded that the temperature variability of the two locations is similar, however deducing the actual temperature behaviour is not possible. Ittoqqortoormiit experiences a temperature variability different to the Renland Ice Cap. Although very closely located, Ittoqqortoormiit is affected by cold sea-ice fog and coastal winds. The Renland peninsula is located within the summer sea-ice free Scoresbysund Fjord which allows summer temperatures to be realtively warm (Cappelen, 2017). Besides, Tasiilaq is not as affected by Icelandic cyclonic activities as other Southeaster Greenland locations and yet influenced by Fram Strait sea-ice export cooling the area throughout the year (Cappelen, 2017). These weather patterns might explain why the Tasiilaq record is a fairly good estimator for the Renland peninsula region.

## 5.3 Performance of Regional Climate Models

Yielding a fair RCM prediction for polar climate is difficult due to various factors. Individual components are not well understood and therefore problematic for the implementation in the RCM. One of the main weaknesses in most polar models is the prognosis of behaviour and extent of sea ice which is important for climatic feedbacks like the albedo. Ice masks are applied to the model domain, in order to account for sea ice and snow. Similarly problematic is the cloud cover prediction, which directly impacts the energy fluxes and determines the probability of precipitation. Since ice retreat, snow melting and precipitation are local processes a high spatial resolution of RCM is favourable. Additionally, small scale site characteristics like elevation, slope and aspect might not be resolved in low resolution model set ups. Contradicting the advantages of a high resolution is the high computational cost that is required for the calculations. Also, some model parameterisations might not be applicable at small scales. Spot evaluation of RCM, like it is performed in this thesis, can therefore provide little insight in the models overall performance unless done with these limitations in mind.

### HIRHAM5

The model predicts colder temperatures than anticipated for the RECAP site. In contrast, the HIRHAM5 model shows a slight positive offset when compared to the Tasiilaq weather station (section 3.4.2). When comparing the site characteristics in the model domain with real values, an elevation discrepancy of 301 m becomes visible (Table 5.2). However, with the HIRHAM5 elevation being lower than in reality,

one would assume the model to show a positive offset compared to the observations. Since this is not the case, elevation corrections can not account for the temperature shift, that is applied in the adjusted HIRHAM5 model run.

TABLE 5.2: Drill site locations in HIRHAM5 model

| site | | latitude °N | longitude °E | elevation m |
|---|---|---|---|---|
| **RECAP** | reality | 71.3036 | -26.7132 | 2331 |
| | HIRHAM5 | 71.2801 | -26.7124 | 2030 |

A temperature shift of 2.08 °C added to each monthly data point yields a graph that shows a warmer summer warming than the one observed. This is due to the fitting technique. Recent temperature fluctuations are higher in amplitude because they have not been diffused as much as earlier temperature signals. Discrepancies between modelled and observed temperatures will therefore be highest in the very top part and since the least square technique weighs every measurement point equally, the model emphasises the fit in the very top part.

### RACMO2.3

Both BTMs were forced with the RACMO2.3 temperature output. For both cases, the model predicts warmer temperatures than would be needed to meet the observed BTC. Again this is contradicting the observations for the Tasiilaq station comparison in section 3.4.2 where the model simulates colder temperatures for Tasiilaq. When comparing the elevations between reality and model (Table 5.3) one finds a difference of 86 m for the RECAP site and 64 m for the old drill site with the model elevation being too low. However, the suggested temperature shifts of -3.58 °C and -4.10 °C are too large in order to be assigned to elevation corrections of the model data. Both the literature lapse rates and the calculated ones yield substantially lower temperature correction values for an elevation difference of <100 m.

TABLE 5.3: Drill site location in RACMO2.3 model

| site | | latitude °N | longitude °E | elevation m |
|---|---|---|---|---|
| **RECAP** | reality | 71.3036 | -26.7132 | 2331 |
| | RACMO2.3 | 71.3091 | -26.7200 | 2245 |
| **Renland 1988** | reality | 71.3064 | -26.7682 | 2340 |
| | RACMO2.3 | 71.3148 | -26.7733 | 2276 |

As can be seen in Figure 3.5 the resolution in the RACMO model is high and the Renland peninsula outlines are well resolved. The allocation of ice and snow

on the Renland peninsula is well resembled in the model domain. Therefore the temperature misfit can not be explained by too coarse grid assumptions.

## 5.4 $\delta^{18}$O as paleothermometer

The resulting BTCs from the model runs with isotope-derived temperatures do not show an ideal match. Yet, the calculated $misfit$-values are very close to the misfits calculated when using actual temperature data as surface forcing. Moreover, the calculated misfits are within the typical uncertainty range of 0.03-0.05 °C (Vinther et al., 2009a). The fact that modelled and measured borehole temperatures diverge questions the validity of the calibrated parameters $c$ and $m$. The found $dT_s/d\delta 18O$ sensitivities of 1.44 °C/‰ (RECAP) and 1.36 °C/‰ (Renland 1988) are lower than other published values. Johnsen, Dansgaard, and White (1989) calculated a sensitivity of 1.5 °C/‰ for the Greenland area, analysing the GISP data from 1971-85 and comparing it to western and southern Greenlandic weather station records. Slightly higher slope values of 1.52-2.22 °C/‰ were found by Cuffey et al. (1994) from the GISP 2 project and 1.67 °C/‰ by Johnsen et al. (1995) from GRIP data. However, those sensitivity values were calibrated to find one universal isotope-temperature dependency for the whole length of the isotope record. Jouzel et al. (1997) pointed out the evidence of spatially and temporally differing slopes. Among the reasons for these findings were changes of precipitation origin, precipitation seasonality and cloud-surface temperature differences. This contradicts the assumption of one paleothermometer calibration that is valid in both glacial and interglacial periods and rejects the previously stated surface temperature/isotope sensitivity values. In order to account for the differences between glacial and interglacial climate and region characteristics, Vinther et al. (2009a) corrected the isotope records of Camp Century, DYE-3, GRIP and NGRIP for elevation changes, accumulation changes and precipitation origin. Hereby, a surface temperature/isotope slope of 2.1 °C/‰ evolve with an average misfit of 0.047 °C. This sensitivity is substantially higher with a higher misfit than is found in this work. When comparing the observed borehole temperature profiles of Camp Century, DYE-3, GRIP and NGRIP to the optimal model fit of Vinther et al. (2009a), it becomes clear that largest discrepancies between observed and modelled temperature curves appear in the uppermost 200 m of the borehole. In fact, it is stated that centennial temperature oscillations contribute the highest uncertainty to the overall misfit. The two Renland boreholes are significantly shorter and the borehole temperature curves can only resolve centennial and higher frequency temperature oscillations. (The 1000 year isotope-derived temperature data set is long enough to force the Renland 1988 model from an isothermal temperature profile to the observed temperature curve - even without a spin-up phase.) The misfit of the Renland models can therefore identify a goodness of fit, comparable to previous works.

Some of the above mentioned obstacles for using $\delta^{18}$O as temperature proxy are

irrelevant for isotope records from the Renland Ice Cap. The ice cap thickness is constrained and therefore constant (Johnsen et al., 1992; Vinther et al., 2009a). In using Holocene data only, the annual accumulation rates are expected to be rather constant. In contradiction to this, the annual layer thicknesses during the Holocene period display no steady decrease but an increase in thickness before 8,000 years b2k in both cores (Fig. 5.1). However, this layer thickness anomaly is assigned to ice flow irregularities and not to increasing amounts of accumulation. Lastly the need to correct for $\delta^{18}$O source content is assumed to be minor since this correction is mainly applied for the transition from glacial to Holocene conditions (Stenni et al., 2004).
Other doubts about the use of isotopes as paleothermometer remain. Isotopes seem to preserve the temperature at the time of snow precipitation, yet they are used as annual mean temperature proxies (Jouzel et al., 1997). It might be that it does not snow in very cold periods biasing the isotope signal to warmer, precipitation rich periods. Furthermore, surface temperatures are inferred from isotopes although the temperature at time of condensation was the cloud temperature. The ratio between cloud and surface temperature is not stable and can not be inferred from isotopes (Johnsen et al., 2001). Although the ice cap thickness has been rather stable, sea level records have revealed that the total elevation of the ice cap surface has changed due to the post-glacial rebound effect after the retreat of the glacial ice sheet. Vinther et al. (2009a) calculated $\delta^{18}$O correction values of up to -0.6 ‰ due to a 100 m past depression uplift of the Renland peninsula since the beginning of the Holocene. Additionally, recent observations provide evidence, that instead of being steady, the isotopic composition of snow alters after deposition (Steen-Larsen et al., 2014). Post depositional processes like air-snow isotope exchange, wind scouring and snow metamorphosis seem to influence the isotope concentrations of the snow layer additionally to temperatures at the time of precipitation (Casado et al., 2016). As previously mentioned, the Renland peninsula frequently experiences melt events. Melted snow, percolating through the snow and refreezing might also influence the Renland isotopic snow composition. Moreover, the water isotope signal is attenuated by water vapour diffusion in the firn column, altering the initial values (Gkinis et al., 2014). This diffusion smoothes the original isotope curve and must be accounted for when translating single isotope values directly. Deconvolution of the original isotope signal using firn diffusion rates as was done by Gkinis et al. (2014) might be necessary before translation. It is not questioned, if snow isotopes carry a temperature signal, merely if a linear formulation of the dependency is the appropriate approach. A different approach for the reconstruction of paleotemperatures is presented in Kindler et al. (2014) by using $^{14}$N-isotopes as temperature-proxy data.

### 5.4.1 The two Holocene temperature records

The vertical offset of the two Holocene temperature histories is likely due to BTM imperfections. The two drill sites are very close and should therefore have experienced the same temperatures. However, since two different linear dependencies had been calculated, this vertical offset is not surprising. The horizontal misalignment instead is due to dating issues. The RECAP core has better identifiable annual layers than the old Renland 1988 core and the dating of the RECAP core is therefore more reliable. This finding has some implications for the flow model of the Renland 1988 site. Half of the used age markers for the Renland flow model lie within the time period 3 ky b2k – 7,2 ky b2k and the good flow model fit should therefore be considered with care. At the same time, the isotopes indicate a very precise dating of the past 3,000 years when the curves show no horizontal offset. Overall, the curve shape follows observations of other literature and proxies. The cold spell events at 8.2 ky b2k (8.2 ka event), 9.3 ky b2k and 11.3 ky b2k are found in the Renland ice cores as well as in all other Greenlandic ice cores (Johnsen et al., 2001; Vinther et al., 2009a). Analyzing the curves for their maximum, the climatic optimum of the Holocene period can be located at around 9 ky b2k. This contradicts other proxies like pollen and sediment cores which predict the optimum conditions in the middle of the Holocene in areas around the Renland Ice Cap (Briner et al., 2016). Central Greenland temperature reconstructions from GRIP and NGRIP show a similar temperature behaviour and the North Canadian Aggasiz ice cap $\delta^{18}$O record is very similar to the Renland records (Johnsen et al., 2001; Vinther et al., 2009a). This would indicate that the Renland peninsula experiences a climate, typical for locations further north. Vinther et al. (2009a) calculated a maximum amplitude of temperature changes throughout the Holocene of almost 6 °C from the Renland 1988 ice core data. Other studies show lower warmest-to-coldest temperature differences of $3\pm1$ °C (Briner et al., 2016). The amplitude from the beginning of the Holocene to the climatic optimum in this thesis lies between those values which is likely due to the omission of the post-glacial rebound effect.

The temperature curves in this study seem to gradually decrease shortly after the 8.2 ka cooling event. This negative trend in temperature since the climatic optimum can be assigned to a gradual decrease in Northern Hemisphere insolation due to Milankovich cycle constellations. However, Monte-Carlo inversions revealed gradual cooling from around 4 ky b2k rather than 8 ky b2k for the GRIP drill site (Dahl-Jensen, 1998). Johnsen et al. (2001) compared six Greenland ice-core records and found similar temperature behaviour in the NGRIP and GRIP isotopes for the Holocene period as in this thesis. No evidence for the temperature history as calculated by the Monte Carlo technique was found in this comparison of isotope-derived temperature reconstructions either. Since the temperature reconstructions from isotopes rely on actual measurements rather than inverse best-guess modelling, this discrepancy is not surprising. BTCs resolve mainly long-term trends. Old annual,

decadal and even centennial temperature oscillations are smoothed out due to diffusion and their records lost. Hence, one borehole temperature curve can be the result of more than one possible climate history (Jouzel et al., 1997). The isotopes preserve high-frequency signals better. However, they are also subject to diffusion (Gkinis et al., 2014). In fitting one smoothed signal to another even more smoothed signal, the precision of the reconstructed temperatures become lower, the further back in time one goes.

Zooming in on the $20^{th}$ century, one can compare the two different temperature reconstruction techniques used in this thesis. The reconstructions using temperature data input and the isotope-derived temperature records do not match completely but have the same overall behaviour. This supports the plausibility of the earlier given Renland temperature history of the past century. A prominent warming can be seen between 1920 and 1960. A steep increase in temperatures can be observed starting around 1980 CE. The gradual cooling seems to have stopped. These observed phenomenons are part of what is widely accepted and referred to as the anthropogenic Climate Change. However, present-day Renland temperatures are about 2 °C colder than the Holocene climatic optimum temperatures.

# Chapter 6

# Conclusion and Outlook

## 6.1 Performance and limitations of the borehole temperature models

The aim of this thesis was to set up a borehole temperature model (BTM) for two Renland sites, in order to estimate the recent climate of the Eastern Greenland peninsula and characterise the ice cap's ice flow. Coupled ice flow-heat transport models, like the one used in this thesis, were successfully set up to model the borehole temperature curves (BTC) at other Greenlandic ice core drill sites. This justified the use of the model approach. However, the hitherto successfully applied Dansgaard-Johnsen *kink-model* could not match the observed ice age markers. Instead, a new flow model assuming a step in the horizontal velocity profile, rather than a kink, performed well for both Renland drill locations. The ice flow was tuned against dated age markers within the ice column and the step-model identified a dead ice layer at both drill site locations. In the case of the Renland 1988 ice core, the herein presented Holocene temperature reconstruction revealed a dating uncertainty between 3.5 and 8 ky b2k. It should therefore be considered to improve the dating of the ice core within that time period.
A Herron-Langway density model was used to incorporate the densification process in the BTM. It produced an acceptable result but leaves some room for improvement. It should be tested if the inclusion of summer melt events in the densification model leads to an improvement of the model fit.
Despite these minor optimisation requirements, the created BTMs simulated BTCs fairly close to the observed temperature profiles. Forcing the model with shifted observed temperature records showed good results with misfits within the typical uncertainty range of 0.03-0.05 °C and lower. Therefore it can be concluded that satisfying ice flow models and BTMs were set up. However, the spatial and temporal validities are limited. The model set up only relies on point measurements which do not necessarily represent the actual average conditions throughout the whole ice cap. Nevertheless, the similarity between the two BTMs indicates a generally consistent ice flow in the plateau region of the ice cap. The herein presented Renland BTMs were designed for Holocene climatic conditions. If a temporal validity extension is desired, the models must be adjusted to account for accumulation rate changes.

Testing the performance of the polar RCM models HIRHAM5 and RACMO2.3 for the Renland region revealed substantial misestimation of surface temperatures. When using the RCM temperature outputs as surface temperature forcing in the BTMs, the time series had to be corrected by a minimum of 2 and up to 4 °C. Again, this is only a point evaluation of the RCM but its conclusion is a poor temperature estimate of the Regional Climate Models for the Renland peninsula.

## 6.2 Renland temperatures of the past century and throughout the Holocene

Temperature reconstruction for the Renland peninsula was performed in two ways. One method made use of actual temperature observations of remote Eastern Greenlandic weather stations. By tuning the Tasiilaq temperature record with the help of ice core borehole temperatures, a Renland temperature record of the 20$^{\text{th}}$ century could be presented. Dominant features of that temperature history are a clearly visible warming between 1925 and 1965 and a significant positive trend in temperatures starting around 1980. Trend analysis of the whole centennial record showed a significant increase of temperatures as well, however with a much lower slope. This observed warming is widely referred to as anthropogenic Climate Change which commenced in the late $19^{th}$-century and is an ongoing process.
The fact that the Tasiilaq temperature record produced a better borehole temperature fit than Denmarkshavn or Ittoqqortoormiit data indicates a Renland climate, which is connected to the South. However, reconstructing one common temperature history for both drill sites from Tasiilaq records was impossible. Optimising the input data for one model resulted in a worse performance of the other model. The suggested Renland temperature history should therefore merely be interpreted as one possible climate scenario.
The second temperature reconstruction method relied on ice core proxy data. Water stable isotopes of the past 1000 years were used as BTM input to formulate the linear relationship between $\delta^{18}$O and annual mean surface temperatures. The calculated $T_s/\delta^{18}$O sensitivities show lower values than other published sensitivities. Subsequent translation of the full isotope records resulted in two Holocene temperature records for the Renland peninsula. Overall, the two temperature curves show a similar shape with small relative horizontal displacements in the mid-Holocene. The climatic optimum is located around 9 ky b2k which is similar to more northern or central-Greenland temperature reconstructions. It is suggested to try non-linear temperature-isotope dependencies and correct the isotope data for smoothing, postglacial rebound effects and moisture origin isotope composition drift. This will also extent the temporal validity of the BTM.

## 6.3 Borehole temperatures - climate proxy and evaluation tool

Ice core borehole temperatures contain a medium intrinsic temperature proxy value. Temperature diffusion eradicates old and high frequency temperature signals. Only the borehole temperature measurements of the upper part of the borehole can be directly used to make quantitative assumptions about the past climate. Nevertheless, BTMs are a powerful tool for the reconstruction of paleotemperatures. By using observed BTCs as desired, optimal BTM outcome, borehole temperatures enable the use of ice core water stable isotope records as temperature proxy. Otherwise, the temperature information stored in heavy isotope concentrations would not be accessible. By finding the dependency between surface temperature and isotope concentrations, the isotopic signals throughout the ice core can be translated into temperature values. With this method, borehole temperatures are indirectly used for the reconstruction of paleotemperatures, dating back hundred thousands of years. However, the difficulty of lost temperature signals due to natural smoothing remains and reconstructed temperatures should be interpreted with care. Even more so, because BTCs are not unambiguous. More than one temperature history can produce the same BTC. When calibrating the paleothermometer, smoothed isotope signals are fitted to smoothed BTCs. By this means, isotope proxy data, that contains high frequency temperature signals is tuned to fit "no-event" borehole temperatures.
Improvements could be achieved when investigating the nature of the relationship between water stable isotopes in snow and surface temperatures. In this thesis, a linear dependency was inferred from the rather stable Holocene climatic conditions. However there is evidence, that the dependency is considerably more complicated.
Since borehole temperatures are a persistent temperature record, they could be implemented in climate modelling. The incorporation of BTMs in isotope enabled GCMs or even in RCMs could act as a validation method provided that the regional ice flow is known.

# Appendix A

# Data correction

## DMI temperature data correction

The Tasiilaq temperature data included 14 missing values. The Ittoqqortoormiit station reported 5 missing values and Danmarkshavn's data had 6 data gaps. The values were linearly interpolated from the enclosing data points for up to three consecutive missing monthly data points. For several consecutive missing months the value were calculated from the mean of the same month of the previous and following year.

## Density data correction

The density at depth 100.375 m in the RECAP data set was calculated as the mean of the two enclosing data points. A density of 905.13 $kg/m^3$ was calculated. The Renland 1988 density data was used down to depth of 101 m.

## Water stable isotope data correction

Missing data in the water stable isotopes measurement was linearly interpolated. 3% of the total amount of 116,143 data points were missing for the RECAP core. The Renland 1988 dataset with 10,458 measurement points was fully available.

# Appendix B

# 3-stage densification model

The model parameters (Table B.1) as well as the corresponding graph (Figure B.1) are given for the 3-stage densification model. A third stage, in the form of Herron-Langway's second stage was added to the original Herron-Langway model.

TABLE B.1: Tuning parameters for 3-stage densification model

| **parameters** | **formula** | **best fit** | **unit** |
|---|---|---|---|
| surface temperature | $T_s$ | -18.4 | °C |
| accumulation rate | $\lambda$ | 0.42 | m w. eq./year |
| initial density | $\rho 0$ | 391.071 | kg/m$^3$ |
| critical density | $\rho_{crit}$ | 497.8113 | kg/m$^3$ |
| transition density | $\rho_{t_{2/3}}$ | 891.325 | kg/m$^3$ |
| fudge factor for K0 | $f0$ | 0.7051 | - |
| fudge factor for K1 | $f1$ | 1.0742 | - |
| fudge factor for K2 | $f2$ | 0.8271 | - |

The density measurements of both drill campaigns were used for the fit. Renland 1988 data was used down to a depth of 100.1 m.

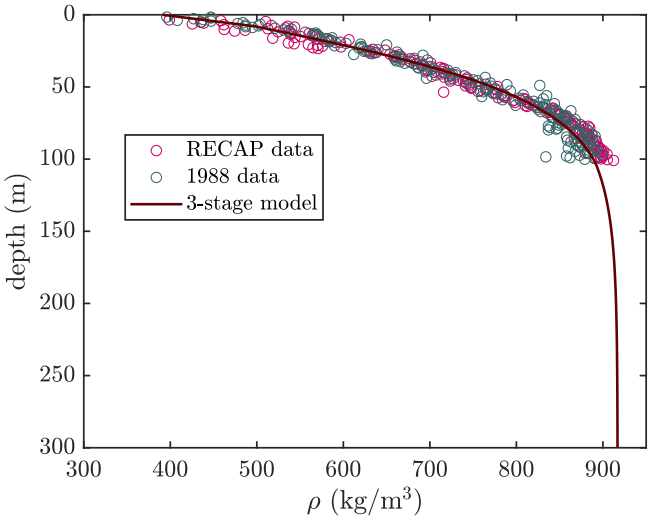


FIGURE B.1: **Three stages densification model with the density data points of both drill campaigns**

# Appendix C

# All ice flow models

The three tested horizontal flow regimes were the original *kink-model* (Figure C.1), the *kink-model* with bottom sliding (Figure C.2) and the step-model (Figure C.3). A combination of each of the models with a dead ice layer was tested as well.

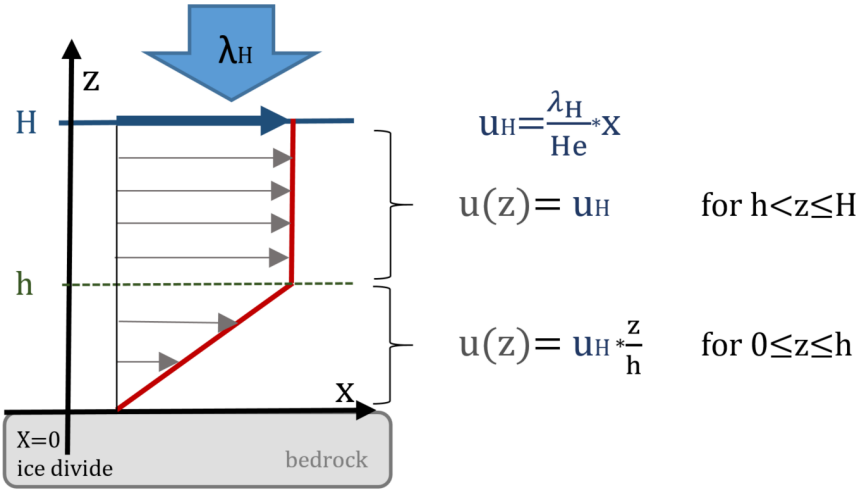


FIGURE C.1: **Scheme for the original *kink-model***
$h$ resembles the kink height.

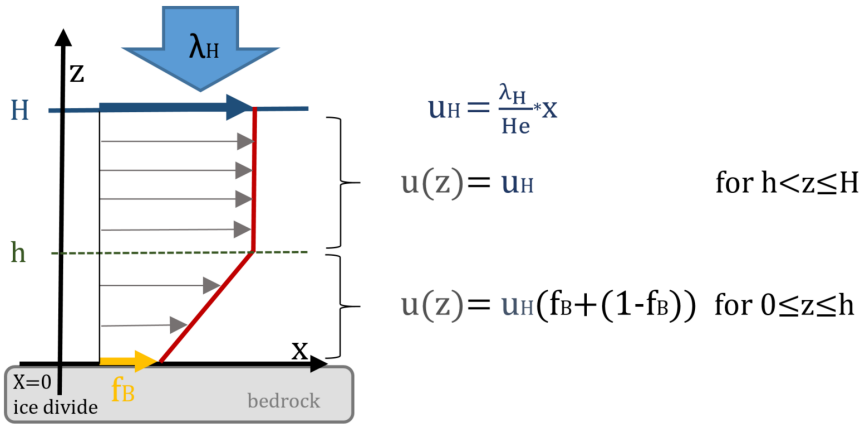


FIGURE C.2: **Scheme for the *kink-model* including bottom sliding**
$h$ resembles the kink height.

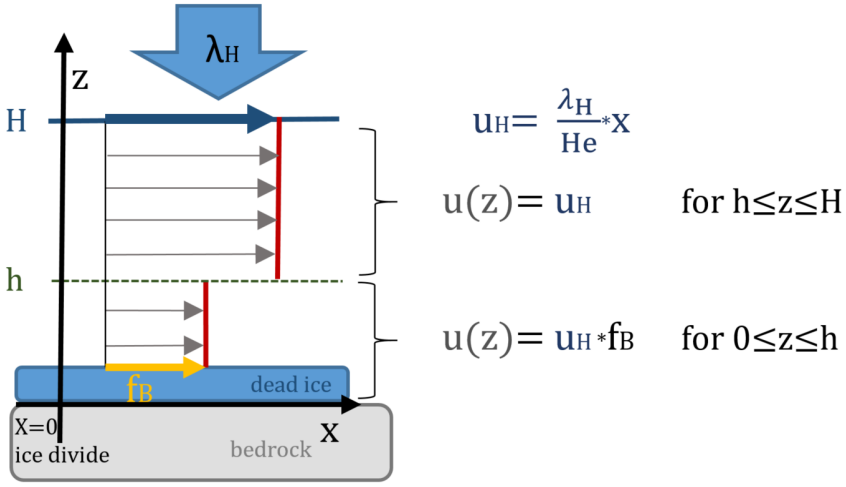


FIGURE C.3: **Scheme for the *step-model***
This schemes includes a dead ice layer. $h$ resembles the step height.

## Renland 1988

Figure C.4 shows the graphical solution of all best-fit flow model results of the Renland 1988 site. The corresponding parameters are presented in Table C.1.

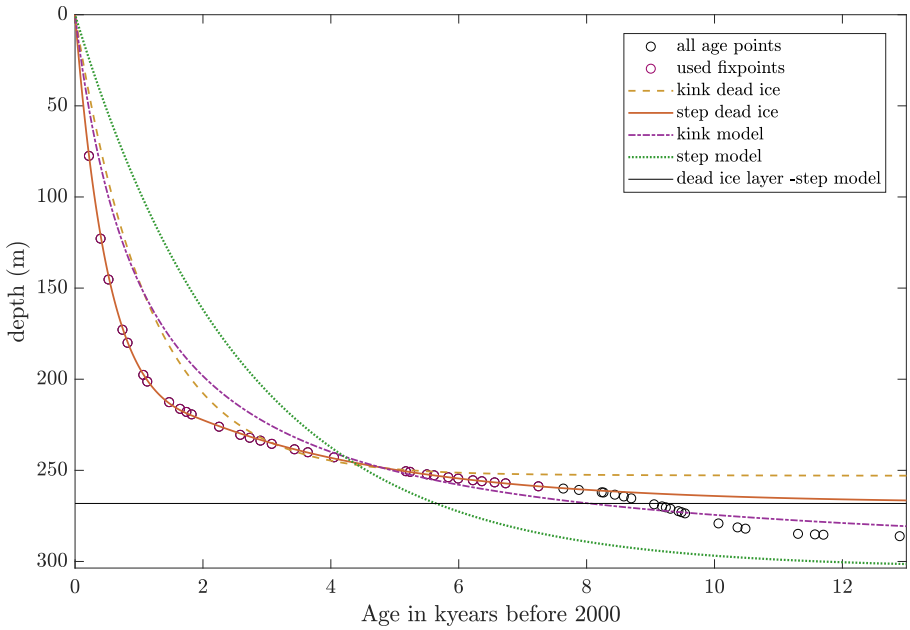


FIGURE C.4: **Different flow model results for the Renland 1988 site**
The *kink-model* with bottom sliding is not shown since the sliding ratio approached zero.

The parameters used for the flow modelling were fitted in an absolute least square sense. The best fit parameters for all models are given in table C.1.

TABLE C.1: Renland 1988 parameters of all tested flow models

| **model** | **dead ice** | **acc. rate** | **step/kink** | **sliding ratio** | **dead ice layer** |
|---|---|---|---|---|---|
| unit | | m ice eq./year | height m | - | m |
| kink | - | 0.29 | 299 | - | - |
| kink-slide | - | 0.29 | 293 | 0.0001 | - |
| step | - | 0.12 | 50 | 0.001 | - |
| kink | ✓ | 0.22 | 51 | - | 50 |
| kink-slide | ✓ | 0.52 | 302 | 0.0003 | 27 |
| step | ✓ | 0.43 | 84 | 0.16 | 35 |
| step* | ✓ | 0.44 | 86 | 0.16 | 36 |

* calculated with minimising $\sum \left( \left( \frac{modelled_i}{observed_i} - 1 \right)^2 \right)$ (relative least square method)

The flow model results for the Renland site differ depending on the amount of age markers used for the fitting. In Figure C.5 two solutions are shown. Displayed are the measured annual layer thicknesses of the Renland 1988 core and the modelled annual layer thicknesses taking into account markers down to a depth of 264 m (red curve) and 280 m (blue curve).

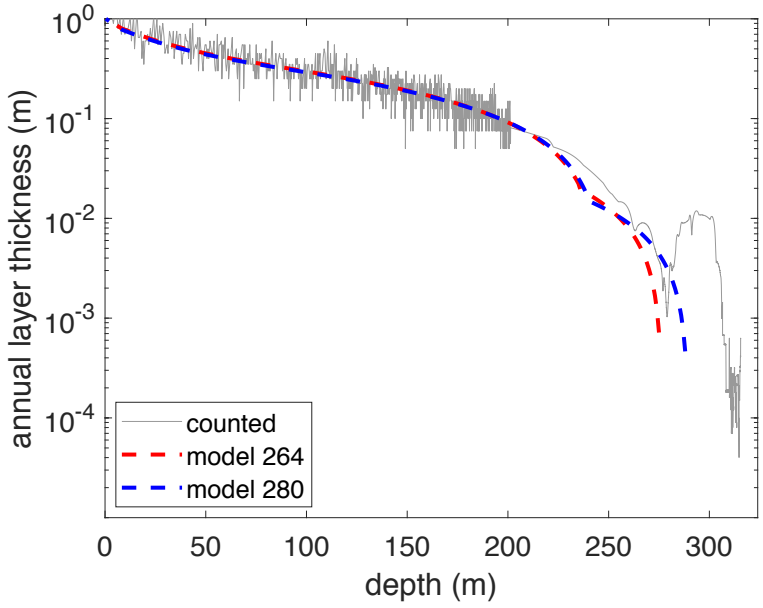


FIGURE C.5: **Two thinning models for the Renland 1988 location** model 264 takes all depth age marker points down to a depth of 264 m into account whereas model 280 uses all marker points down to 280 m.

## RECAP

Figure C.6 shows the graphical solution of all best-fit flow model results of the RECAP site. The corresponding parameters are presented in Table C.2.

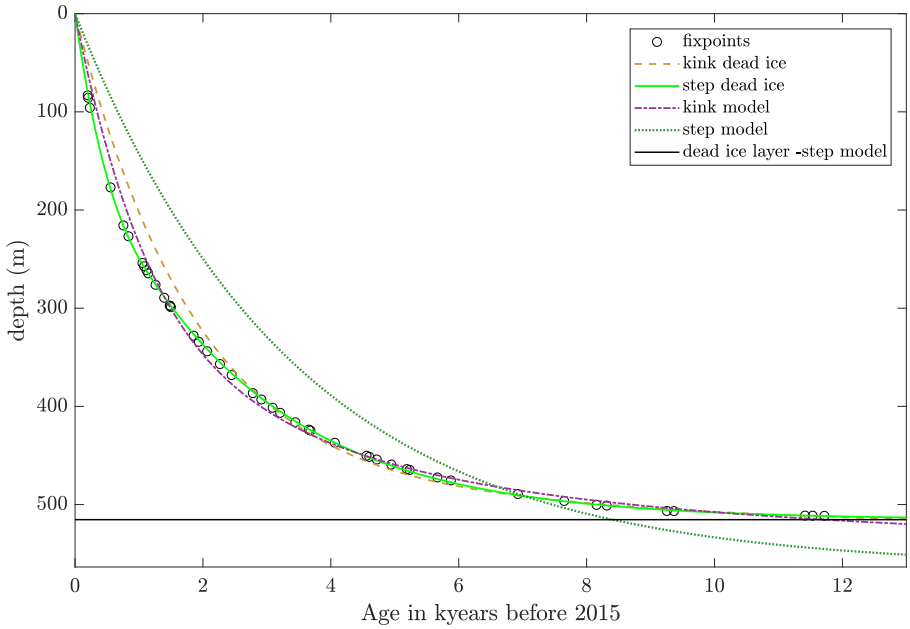


FIGURE C.6: **Different flow model results for the RECAP site** The *kink-model* with bottom sliding is not shown since the sliding ratio approached zero.

The parameters used for the flow modelling were fitted in an absolute least square sense. The best fit parameters for all models are given in table C.2.

TABLE C.2: RECAP parameters of all tested flow models

| **model** | **dead ice** | **acc. rate** | **step/kink** | **sliding ratio** | **dead ice layer** |
|---|---|---|---|---|---|
| unit | | m ice eq./year | height m | - | m |
| kink | - | 0.33 | 217 | - | - |
| kink-slide | - | 0.33 | 217 | 0.0001 | - |
| step | - | 0.17 | 1 | 0.0001 | - |
| kink | ✓ | 0.26 | 91 | - | 27 |
| kink-slide | ✓ | 0.35 | 563 | 0.3 | 46 |
| step | ✓ | 0.46 | 305 | 0.29 | 48 |
| step* | ✓ | 0.48 | 310 | 0.27 | 48 |

* calculated with minimising $\sum \left( \left( \frac{modelled_i}{observed_i} - 1 \right)^2 \right)$ (relative least square method)

Table C.3 contains the trend analysis results of the Renland monthly temperature time series. The temperature time series was created from the Tasiilaq temperature record applying a temperature shift of -17.35 °C. The trend analysis was performed using the Mann-Kendall test for monotonic trends and Sen's slope estimate to estimate the temperature increase.

| period | month | Mann-Kendall parameter | Significance of trend | Sen's slope | lower limit 95% conf. interval | upper limit 95% conf. interval |
|---|---|---|---|---|---|---|
| **1895-2015** | january | 2.75 | ○○ | 0.021 | 0.007 | 0.037 |
| | february | 3.49 | ○○○ | 0.030 | 0.014 | 0.045 |
| | march | 1.25 | | 0.009 | -0.005 | -0.22 |
| | april | 1.85 | + | 0.010 | 0.000 | 0.020 |
| | may | 0.13 | | 0.000 | -0.006 | 0.007 |
| | june | -1.98 | ○ | -0.006 | -0.011 | 0.000 |
| | july | -0.26 | | 0.000 | -0.006 | 0.005 |
| | august | 3.09 | ○○ | 0.007 | 0.003 | 0.012 |
| | september | 2.23 | ○ | 0.007 | 0.000 | 0.013 |
| | october | 2.21 | ○ | 0.009 | 0.000 | 0.017 |
| | november | 3.62 | ○○○ | 0.018 | 0.008 | 0.027 |
| | december | 1.48 | | 0.010 | -0.003 | 0.023 |
| | annual | 3.51 | ○○○ | 0.010 | 0.005 | 0.015 |
| **1895-1987** | january | 1.19 | | 0.015 | -0.011 | 0.040 |
| | february | 2.41 | ○ | 0.033 | 0.007 | 0.058 |
| | march | 0.41 | | 0.005 | -0.018 | 0.026 |
| | april | 0.97 | | 0.007 | -0.007 | 0.024 |
| | may | 0.15 | | 0.000 | -0.011 | 0.012 |
| | june | -2.52 | ○ | -0.010 | -0.017 | -0.002 |
| | july | -1.30 | | -0.005 | -0.014 | 0.002 |
| | august | 0.99 | | 0.003 | -0.003 | 0.010 |
| | september | 0.14 | | 0.000 | -0.008 | 0.009 |
| | october | 1.22 | | 0.008 | -0.004 | 0.022 |
| | november | 1.02 | | 0.009 | -0.007 | 0.025 |
| | december | -0.73 | | -0.006 | -0.025 | 0.013 |
| | annual | 1.15 | | 0.004 | -0.004 | 0.013 |
| **1988-2015** | january | 3.50 | ○○○ | 0.191 | 0.085 | 0.273 |
| | february | 2.22 | ○ | 0.127 | 0.017 | 0.242 |
| | march | 2.93 | ○○ | 0.153 | 0.075 | 0.235 |
| | april | 1.64 | | 0.078 | -0.008 | 0.174 |
| | may | 2.26 | ○ | 0.050 | 0.006 | 0.092 |
| | june | 2.81 | ○○ | 0.077 | 0.032 | 0.125 |
| | july | 2.48 | ○ | 0.054 | 0.011 | 0.094 |
| | august | 2.49 | ○ | 0.059 | 0.020 | 0.106 |
| | september | 3.11 | ○○ | 0.082 | 0.033 | 0.145 |
| | october | 0.97 | | 0.028 | -0.025 | 0.089 |
| | november | 0.30 | | 0.009 | -0.049 | 0.066 |
| | december | 1.70 | + | 0.100 | -0.019 | 0.200 |
| | annual | 4.32 | ○○○ | 0.091 | 0.058 | 0.120 |

# Bibliography

Alley, Richard B. et al. (2010). "History of the Greenland Ice Sheet: paleoclimatic insights". In: *Quaternary Science Reviews* 29.15-16, pp. 1728–1756. DOI: 10.1016/J.QUASCIREV.2010.02.007.

Briner, Jason P. et al. (2016). *Holocene climate change in Arctic Canada and Greenland*. DOI: 10.1016/j.quascirev.2016.02.010.

Buchardt, Susanne Lilja (2009). "Basal melting and Eemian ice along the main ice ridge in northern Greenland". PhD Thesis. Copenhagen University, p. 199.

Cappelen, John (DMI) (2017). *Greenland - DMI Historical Climate Data Collection 1784-2016*. Tech. rep. Danish Meterological Institute, p. 108.

Casado, Mathieu et al. (2016). "Archival of the water stable isotope signal in East Antarctic ice cores". In: *The Cryosphere Discussions*, pp. 1–33. DOI: 10.5194/tc-2016-263.

Christensen, Ole Bøssing et al. (2007). "The HIRHAM Regional Climate Model". In:

Crank, J and P Nicolson (1996). "A practical method for numerical evaluation of solutions of partial differential equations of the heat-conduction type". In: *Advances in Computational Mathematics* 6, pp. 207–226.

Cuffey, K.M. and W.S.B. Paterson (2010). *The Physics of Glaciers -4th ed*. 4th Editio. Elsevier, p. 681. ISBN: 978-0-12-369461-4.

Cuffey, Kurt M. et al. (1994). "Calibration of the $\delta$18O isotopic paleothermometer for central Greenland, using borehole temperatures". In: *Journal of Glaciology* 40.135, pp. 341–349. DOI: 10.3189/S0022143000007425.

Dahl-Jensen, D. (1998). "Past Temperatures Directly from the Greenland Ice Sheet". In: *Science* 282.5387, pp. 268–271. DOI: 10.1126/science.282.5387.268.

Dahl-Jensen, Dorthe et al. (2003). "Basal melt at NorthGRIP modeled from borehole, ice-core and radio-echo sounder observations". In: *Annals of Glaciology* 37, pp. 207–212. DOI: 10.3189/172756403781815492.

Dansgaard, W (1964). "Stable isotopes in precipitation". In: *Tellus* 16. DOI: 10.1111/j.2153-3490.1964.tb00181.x.

Dansgaard, W and Sigfùs J. Johnsen (1969). "A flow model and a time scale for the ice core from camp century, Greenland". In: *JOurnal of Glaciology* 8.53.

Dee, D. P. et al. (2011). "The ERA-Interim reanalysis: configuration and performance of the data assimilation system". In: *Quarterly Journal of the Royal Meteorological Society* 137.656, pp. 553–597. DOI: 10.1002/qj.828.

Erokhina, Olga et al. (2017). "Dependence of slope lapse rate over the Greenland ice sheet on background climate". In: *Journal of Glaciology* 63.239, pp. 568–572. DOI: 10.1017/jog.2017.10.

Gilbert, R.O. (1987). *Statistical methods for environmental pollution monitoring*.

Gkinis, V. et al. (2014). "Water isotope diffusion rates from the NorthGRIP ice core for the last 16,000 years – Glaciological and paleoclimatic implications". In: *Earth and Planetary Science Letters* 405, pp. 132–141. DOI: 10.1016/j.epsl.2014.08.022.

Grootes, P. M. et al. (1993). "Comparison of oxygen isotope records from the GISP2 and GRIP Greenlandice cores". In: *Nature* 366.6455, pp. 552–554. DOI: 10.1038/366552a0.

Gundestrup, N.S et al. (1993). "Bore-hole survey at Camp Century, 1989". In: *Cold Regions Science and Technology* 21.2, pp. 187–193. DOI: 10.1016/0165-232X(93)90006-T.

Hanna, Edward et al. (2005). "Runoff and mass balance of the Greenland ice sheet: 1958–2003". In: *Journal of Geophysical Research* 110.D13, p. D13108. DOI: 10.1029/2004JD005641.

Herron, Michael M and Chester C Langway (1980). "FIRN DENSIFICATION: AN EMPIRICAL MODEL". In: *Journal of Glaciology* 25.93. DOI: 10.1017/S0022143000015239.

Huybrechts, P et al. (2007). "Ice thinning, upstream advection, and non-climatic biases for the upper 89% of the EDML ice core from a nested model of the Antarctic ice sheet". In: *Clim. Past* 3, pp. 577–589.

Intergovernmental Panel on Climate Change, ed. (2014). *Climate Change 2013 - The Physical Science Basis*. Cambridge: Cambridge University Press. ISBN: 9781107415324. DOI: 10.1017/CBO9781107415324.

Johannessen, Ola M. et al. (2004). "Arctic climate change: Observed and modelled temperature and sea-ice variability". In: *Tellus, Series A: Dynamic Meteorology and Oceanography* 56.4, pp. 328–341. DOI: 10.1111/j.1600-0870.2004.00060.x.

Johnsen, S. J., W. Dansgaard, and J. W. C. White (1989). "The origin of Arctic precipitation under present and glacial conditions". In: *Tellus B* 41B.4, pp. 452–468. DOI: 10.1111/j.1600-0889.1989.tb00321.x.

Johnsen, Sigfus et al. (1995). "Greenland paleotemperatures derived from GRIP bore hole temperature and ice core isotope profiles". In: *TELLUS* 47B, pp. 624–629.

Johnsen, Sigfùs J. (1977). "Stable isotope profiles compared with temperature profiles in firn with historical temperature records". In: *Isotopes and Impurities in Snow and Ice - Symposium 118*, pp. 338–392.

Johnsen, Sigfùs J. et al. (1992). "A "deep" ice core from East Greenland". In: *Meddelelser om Gronland, Geoscience* 29, pp. 3–22.

Johnsen, Sigfus J. et al. (2001). "Oxygen isotope and palaeotemperature records from six Greenland ice-core stations: Camp Century, Dye-3, GRIP, GISP2, Renland and

NorthGRIP". In: *Journal of Quaternary Science* 16.4, pp. 299–307. DOI: 10.1002/jqs.622.

Jouzel, J. et al. (1997). "Validity of the temperature reconstruction from water isotopes in ice cores". In: *Journal of Geophysical Research: Oceans* 102.C12, pp. 26471–26487. DOI: 10.1029/97JC01283.

Jouzel, J. et al. (2007). "Orbital and Millennial Antarctic Climate Variability over the Past 800,000 Years". In: *Science* 317.5839, pp. 793–796. DOI: 10.1126/science.1141038.

Kalnay, Eugenia (2003). *Atmospheric modeling, data assimilation, and predictability*. Cambridge University Press, p. 341. ISBN: 9780521796293.

Kawamura, Kenji et al. (2017). "State dependence of climatic instability over the past 720,000 years from Antarctic ice cores and climate modeling". In: *Science Advances* 3.2, e1600446. DOI: 10.1126/sciadv.1600446.

Kindler, P. et al. (2014). "Temperature reconstruction from 10 to 120 kyr b2k from the NGRIP ice core". In: *Climate of the Past* 10.2, pp. 887–902. DOI: 10.5194/cp-10-887-2014.

NEEM (2013). "Eemian interglacial reconstructed from a Greenland folded ice core". In: *Nature* 493.7433, pp. 489–494. DOI: 10.1038/nature11789.

Noël, Brice et al. (2016). "A daily, 1 km resolution data set of downscaled Greenland ice sheet surface mass balance (1958–2015)". In: *The Cryosphere* 10.5, pp. 2361–2377. DOI: 10.5194/tc-10-2361-2016.

Noël, Brice et al. (2017). "Modelling the climate and surface mass balance of polar ice sheets using RACMO2, Part 1: Greenland (1958–2016)". In: *The Cryosphere Discussions*, pp. 1–35. DOI: 10.5194/tc-2017-201.

Nye, J. F. (1951). "The Flow of Glaciers and Ice-Sheets as a Problem in Plasticity". In: *Proceedings of the Royal Society A: Mathematical, Physical and Engineering Sciences* 207.1091, pp. 554–572. DOI: 10.1098/rspa.1951.0140.

Nye, J F (1952). "THE MECHANICS OF GLACIER FLOW". In: *Journal of Glaciology* 2.11, pp. 52–53.

Petit, J. R. et al. (1999). "Climate and atmospheric history of the past 420,000 years from the Vostok ice core, Antarctica". In: *Nature* 399.6735, pp. 429–436. DOI: 10.1038/20859.

PGC (2017). "Guide: Introduction to ArcticDEM". In: *Polar Geospatial Center*.

Rasmussen, S. O. et al. (2006). "A new Greenland ice core chronology for the last glacial termination". In: *Journal of Geophysical Research* 111.D6, p. D06102. DOI: 10.1029/2005JD006079.

Reeh, Niels et al. (2005). "An empirical firn-densification model comprising ice lenses". In: *Annals of Glaciology*. Vol. 42, pp. 101–106. ISBN: 1727564057. DOI: 10.3189/172756405781812871.

Schytt, V (1958). "Glaciology II A: Snow studies at maudheim. Glaciology. B:Snow studies inland. Glaciology C: The inner structure of the ice shelf at Maudheim as

shown by core drilling." In: *Norwegian-British-Swedish-Antarctic Expedition 1949-52. Scientific Results.* IV.

Sigl, M et al. (2015). "Timing and climate forcing of volcanic eruptions for the past 2,500 years". In: *Nature* 523.7562, pp. 543–549. DOI: 10.1038/nature14565.

Steen-Larsen, H C et al. (2014). "What controls the isotopic composition of Greenland surface snow?" In: *Clim. Past* 10, pp. 377–392. DOI: 10.5194/cp-10-377-2014.

Steffen, Konrad and Jason Box (2001). "Surface climatology of the Greenland Ice Sheet: Greenland Climate Network 1995–1999". In: *Journal of Geophysical Research: Atmospheres (1984–2012)* 106.D24, pp. 33951–33964. DOI: 10.1029/2001JD900161.

Stenni, B. et al. (2004). "A late-glacial high-resolution site and source temperature record derived from the EPICA Dome C isotope records (East Antarctica)". In: *Earth and Planetary Science Letters* 217.1-2, pp. 183–195. DOI: 10.1016/S0012-821X(03)00574-0.

Utrecht University (2018). *Ice and Climate : Regional modelling*. (Visited on 01/20/2018).

Vinther, B. M. *The REnland ice CAP project (Sapere Aude)*.

Vinther, B. M. et al. (2008). "Synchronizing ice cores from the Renland and Agassiz ice caps to the Greenland Ice Core Chronology". In: *Journal of Geophysical Research Atmospheres* 113.8, p. D08115. DOI: 10.1029/2007JD009143.

Vinther, B. M. et al. (2009a). "Holocene thinning of the Greenland ice sheet". In: *Nature* 461.7262, pp. 385–388. DOI: 10.1038/nature08355.

— (2009b). "Holocene thinning of the Greenland ice sheet - supplementary information". In: *Nature* 461.7262. DOI: 10.1038/nature08355.

Weller, Gunter and Peter Schwerdtfeger (1970). "Thermal Properties and Heat Transfer Processes of Low-Temperature Snow". In: pp. 27–34. DOI: 10.1002/9781118664872.CH3.